NANOHARDNESS TESTING OF MULTIPHASE C-Mn-Si STEEL

MÁRIA MOLNÁROVÁ[a], PETRA GAVENDOVÁ[a], TIBOR KVAČKAJ[b], and FRANTIŠEK KOVÁČ[a]

[a] *Institute of materials research, Slovak academy of sciences, 040 01 Košice,* [b] *Department of Metals Forming, Faculty of Metallurgy, Technical University of Košice, 042 00 Košice, Slovakia*
mariamolnarova@gmail.com

Keywords: nanohardness, transformation induced plasticity, ferrite, austenite, bainite

1. Introduction

TRIP (transformation induced plasticity) steels were introduced by Zackay et al.[1] in austenitic stainless steels in 1967, describing how the transformation supports „high-strength steels toughness improving“. After[2–4] the aspect of TRIP steels originates from a phase transformation of metastable austenite into much harder martensite during deformation[5], and must provide ferrite formation and saturation of austenite (RA) solid solution by carbon without possibility of pearlite and cementite formation, which can be suppressed by rapid cooling rate and elements addition like Si, Cr or Mn[6]. After Wu et al.[7] rapid cooling is necessary for preventing the relaxation after deformation, so more dislocations stay retained after several step cooling at room temperature. Tsusaki and Raghavan[8] found that a large dislocation density hinders a growth of martensitic plates. The stability of RA against the martensitic transformation is improved by increasing dislocation density[9]. There are few reports on the mechanical behaviour of different phases in multiphase TRIP steels due to the difficulty of making such small-scale measurements, especially in individual austenite grains[10]. The nanoindentation method, developed by Oliver and Pharr[11], can provide information about the mechanical behaviour when material is being deformed at the sub-micron scale[12].

For this contribution multiphase steel with composition of C 0.18wt.%, Mn 1.47wt.%, Si 1.8wt.%, P 0.015wt.%, S 0.007wt.%, Cu 0.06wt.%, Ni 0.04wt.%, Cr 0.06wt.%, $Al_{tot.}$ 0.028wt.%, Nb 0.005wt.%, Sn 0.007wt.% was investigated for the dependence of nanohardness in different phases on intercritical annealing temperature 540–740 °C and subsequent austempering temperature 350–450 °C.

2. Material and methods

Two groups of steel samples after two step deformation (50 %) were used for investigation of influence of annealing parameters on nanohardness in different structure phases. First group was processed by intercritical annealing (T_{IC} = 540–740 °C) and austempering (T_A = 350–450 °C), where the samples were air-cooled after each processing step down to room temperature (SA). Second group was processed by intercritical annealing (T_{IC} = 540–740 °C) and austempering (T_A = 350–450 °C), where the samples were cooled to T_{IC} by double water jet and air-cooled before and after austempering down to room temperature (QA).

Structure of the samples cooled only in air consisted of ferrite (F), martensite/martnesite+bainite (M+B), pearlite (P) formed at specific isothermal conditions at cca 600 °C and low cooling rates also occurs[13], see Fig. 1. The other group of samples is characterized by the structure F+(M+B) / F+P. Retained austenite was expected in the islands of (M+B) inside original austenite grains bouded by F, see Fig. 2.

Nanohardness testing was performed by Nanoindenter G200 with Berkovich tip indenter using depth control system. Parameters of measurements were as follows: maximum depth h_{max}= 600 nm, the Poisson´s ratio

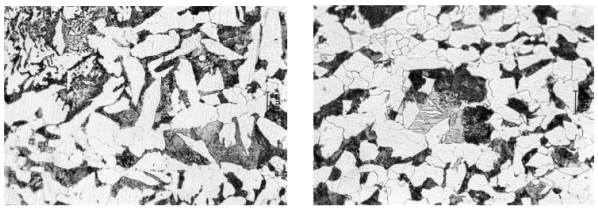

SA1.1 660°C/40s; 400°C/300s;X_F=56%,1000x **SA1.2** 600°C/180s; 400°C/300s;X_F=60%,1000x

Fig. 1. **Structure of selected samples air-cooled**

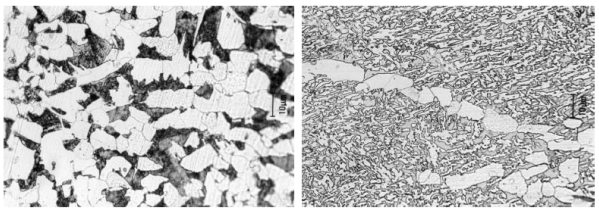

QA1.1 740°C/20s;400°C/300s;X_F=61%,1000x **QA1.2** 570°C/120s;400°C/300s;X_F=48%,1000x

Fig. 2. **Structure of selected samples cooled on air and by double water jet**

s = 0.3, peak holding time 10 s. After reaching the maximum depth the nanohardness was measured in different phases (F, B+M mixture) during the holding time.

3. Results and discussion

Fig. 3 shows indentation curves of average values of different phases. As one can see, there is the difference in hardness values between the phases Fig. 2. Not only due to fraction and morphology of each phase, but also due to different annealing parameters[14] (intercritical annealing and austempering). The indentation hardness reached the values of cca 4 GPa for ferrite and cca 5.5 GPa for mixture of samples cooled by water jet before austempering. Samples cooled only on air reached the values of indentation hardness of cca 3.5 GPa for ferrite and cca 5.5 GPa for mixture.

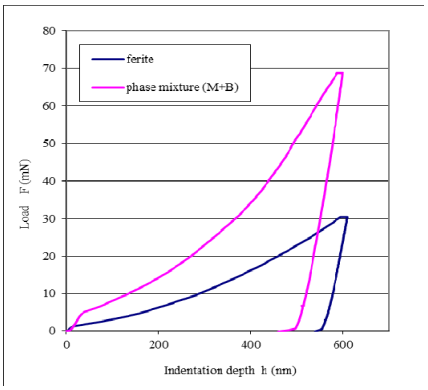

Fig. 3. **Indentation curves of different phases – ferrite (pink), martensite + bainite mixture (blue)**

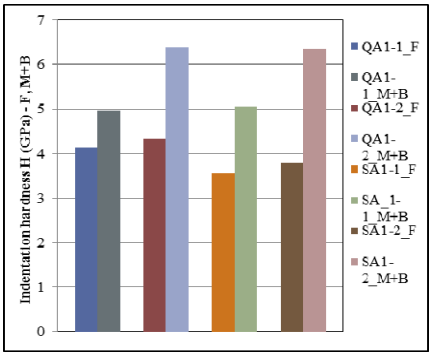

Fig. 4. **Indentation hardness values of selected samples phases influenced by annealing parameters**

4. Conclusions

The local determination of indentation hardness of the investigated multiphase steel revealed differences in the individual phases due to volume fraction and morphology of each phase, and also due to different annealing parameters during controlled rolling.

This work was supported by the Scientific Grant Agency of Slovak republic as a grant project VEGA No. 2 / 0138 / 10. This work was realized within the frame of the project „New Materials and Technologies for Energetics"(ITMS: 26220220061), which is supported by the Operational Program "Research and Development" financed through European Regional Development Fund.

REFERENCES

1. Zackay V. F., Parker E. R., Fahr D.: Trans. ASM *60*, 252 (1967).
2. Olson G. B., Cohen M.: Metall. Trans. A *13*, 1907 (1982).
3. Zaefferer S., Ohlert J., Bleck W.: Acta Mater. *52*, 2765 (2004).
4. Han H. N., Oh C.-S., Kim G., Kwon O.: Mater. Sci. Eng. A-Struct *499*, 462 (2009).
5. Quade H., Prahl U., Bleck W.: Chem. Listy *105*, s705 (2011).
6. Kvackaj T., et al.: Acta Metall. Slovaca *16*, 268 (2010).
7. Wu D., Li Z., Lü H.-S.: J. Iron Steel Res. Int. *15*, 65 (2008).
8. Stephane G., Philippe H., Francis D.: Steel Res. *73*, 280 (2002).
9. Timokhina I. B., Pereloma E. V.: Mater. Sci. Technol. *17*, 135 (2001).
10. Ahn T.-H., et al.: Scripta Mater. *63*, 540 (2010).
11. Oliver W. C., Pharr G. M.: J. Mater. Res. *19*, 3 (2004).
12. Rodríguez R., Gutierrez I.: Mater. Sci. Eng. A-Struct *361*, 377 (2003).
13. Molnárová M., et al.: Chem. Listy *104*, s353 (2010).
14. Némethová L., Kvačkaj T., Mišičko R., Pokorný I., Kovárová I.: Acta Metall. Slovaca *3*, 173 (2009).

M. Molnárová[a], P. Gavendová[a], T. Kvačkaj[b], and F. Kováč[a] *(Institute of materials research, Slovak Academy of Sciences, Košice, [b] Dpt. of Metals Forming, Faculty of Metallurgy, Technical University of Košice, Košice, Slovakia):* **Nanohardness Testing of Multiphase C-Mn-Si Steel**

This paper deals with investigation of the dependence of nanohardness in C-Mn-Si steel different structure phases on intercritical annealing temperature 540–740 °C and subsequent austempering temperature 350–450 °C. There are few reports on the mechanical behaviour of different phases in multiphase TRIP steels due to the difficulty of making such small-scale measurements, especially in individual austenite grains[10]. The nanoindentation method, developed by Oliver and Pharr[11], can provide information about the mechanical behaviour when material is being deformed at the sub-micron scale[12].

UP-SCALING MICROLEVEL ELASTIC PROPERTIES OF HETEROGENEOUS STRUCTURAL MATERIALS

JIŘÍ NĚMEČEK, VLASTIMIL KRÁLÍK, and JAROSLAV VONDŘEJC

Czech Technical University in Prague, Thákurova 7, 166 29 Prague 6, Czech Republic
jiri.nemecek@fsv.cvut.cz

Keywords: micromechanics, nanoindentation, heterogeneous materials, up-scaling, Mori-Tanaka, FFT

1. Introduction

Structural materials such as concrete, gypsum, plastics, wood or metals are characterized by a multiscale heterogeneity at different length scales (nm−m). Their mechanical properties are often assessed from macroscopic tests on large scale samples that can only describe overall (averaged) properties like overall Young's modulus or strength. Nowadays, it is possible to access also lower material levels and small-scale properties of individual material components experimentally e.g. by nanoindentation.

Wide theoretical background has also been laid in the field of micromechanics together with the development of classical composites. Micromechanical approaches are applied for matrix-inclusion problems to search for effective properties of the whole representative volume element – RVE[1–3]. Although, the theoretical development in micromechanics is tremendous the knowledge of the material microstructure and its micromechanical properties is the key factor in obtaining relevant results.

In this paper, we deal with the micromechanical prediction of the effective elastic properties for several structural materials on a scale of several hundreds of micrometers. Simple analytical and more complex numerical approaches are utilized.

2. Methods

Microscale experimental measurements, e.g. nanoindentation, can supply valuable data on mechanical properties of small material volumes or even distinct material phases in multi-phase materials. The size of RVE in a multi-scale material is considered so that it is much larger than the smallest microstructural inhomogeneity but it is small enough to represent the whole material level. Then, the up-scaling methodology can be summarized in the following main steps:

- Definition of scales in the material (i.e. RVE size definition for each scale).
- Nanoindentation on distinct material phases and characterization of their volume fractions within RVE.
- Applying homogenization techniques to assess effective RVE properties.

For heterogeneous structural materials, the task of finding number of mechanically distinct microstructural phases, their mechanical properties and volume fractions, can be solved by nanoindentation. To access distinct phases, the size of individual indents h have to be considerably smaller than the dimension of the studied phase d (i.e. $h<<d$). Such assumption is especially important in multi-phase to avoid phase interactions[4,5]. As a rule of thumb $h<d/10$ is usually used[4]. Also, special approaches like massive grid indentation[4] or statistical deconvolution[4,6,7] can be utilized in solving this task.

3. Homogenization

In general, homogenization methods search for effective composite properties. Analytical schemes often rely on simplified assumptions concerning inclusion geometry, boundary conditions or isotropy. More complex results can be obtained from numerical methods that are based on finite element solution or fast Fourier transformation, for instance.

The classical solution based on constant stress/strain fields in individual microscale components for ellipsoidal inclusion embedded in an infinite body was derived by Eshelby[2]. Effective elastic properties are then obtained through averaging over the local contributions. Various estimates considering different geometrical constraints or special choices of the reference medium known as rule of mixtures, Voight and Reuss bounds, Mori-Tanaka method or self-consistent scheme[1–3] can be used. For the case of a composite material with prevailing matrix and spherical inclusions the Mori-Tanaka method[3] was previously found to be simple but powerful tool to estimate effective composite properties also for structural materials[4] and, therefore, it was used in this paper. In the Mori-Tanaka method, the homogenized isotropic bulk and shear moduli of an r-phase composite are assessed as follows:

$$k_{\mathrm{hom}}=\frac{\sum_r f_r k_r (1+\alpha_0(\frac{k_r}{k_0}-1))^{-1}}{\sum_r f_r (1+\alpha_0(\frac{k_r}{k_0}-1))^{-1}} \tag{1}$$

$$\mu_{\mathrm{hom}}=\frac{\sum_r f_r \mu_r (1+\beta_0(\frac{\mu_r}{\mu_0}-1))^{-1}}{\sum_r f_r (1+\beta_0(\frac{\mu_r}{\mu_0}-1))^{-1}} \tag{2}$$

$$\alpha_0 = \frac{3k_0}{3k_0 + 4\mu_0}, \quad \beta_0 = \frac{6k_0 + 12\mu_0}{15k_0 + 20\mu_0} \tag{3}$$

where the subscript 0 corresponds to the reference medium and r corresponds to a particulate inclusion. Thus, k_0 and μ_0 are the bulk and shear moduli of the reference medium, while k_r and μ_r refer to the inclusion phases. Further, bulk and shear moduli can be recomputed to engineering values of Young's modulus and Poisson's ratio as:

$$E = \frac{9k\mu}{3k + \mu}, \quad \nu = \frac{3k - 2\mu}{6k + 2\mu} \tag{4}$$

Local strain and stress fields in a RVE can also be found by numerical methods like finite element method or method based on fast Fourier transformation (FFT). The former one was proved to be reliable and computationally inexpensive method which only utilizes mechanical data in the discretization (grid) points. Such a concept perfectly matches with the concept of the grid nanoindentation. Therefore, the FFT method was chosen for our purposes. The numerical scheme used here solves the problem of finding the effective elasticity tensor with a periodically repeating RVE by using discretization of an integral Lippmann–Schwinger equation:

$$\boldsymbol{\varepsilon}(\mathbf{x}) = \mathbf{e}^0 - \int_\Omega \Gamma^0(\mathbf{x}-\mathbf{y}) : (\mathrm{L}(\mathbf{y}) - \mathrm{L}^0) : \boldsymbol{\varepsilon}(\mathbf{y}) d\mathbf{y} \tag{5}$$

in which $\boldsymbol{\varepsilon}$ and L stand for the local (inhomogeneous) strain and stiffness tensor, respectively, and $\mathbf{e}^0$ is the homogenized strain defined as a spatial average over RVE domain Ω as

$$\mathbf{e}^0 = \langle \boldsymbol{\varepsilon} \rangle = \frac{1}{\Omega} \int_\Omega \boldsymbol{\varepsilon}(\mathbf{x}) d\mathbf{x} \tag{6}$$

Γ^0 is the periodic Green operator associated with the reference medium and L^0 in Eq. (*5*) stands for a reference elasticity tensor, which is a parameter of the method proposed by Moulinec and Suquet[8]. The problem is further discretized in the Fourier space. This leads to the solution of a nonsymmetric linear system of equations, which can be effectively treated by e.g. the conjugate gradient method (Zeman et.al.[9]).

4. Experimental program

Three types of heterogeneous structural materials were selected for this work: cement paste, gypsum and aluminium alloy.

Cement paste samples were prepared from Portland cement CEM-I 42,5 R with water to cement weight ratio equal to 0.5 and stored in water for several years[10]. Therefore, high degree of hydration can be anticipated in the samples. The microstructure of cement paste includes several major chemical phases, namely the hydration products: calcium-silica hydrates (C-S-H), calcium hydroxide $Ca(OH)_2$, residual clinker and the porosity.

Dental gypsum (Interdent®) was chosen as a model system for gypsum based materials[11]. Samples were prepared with water to gypsum ratio 0.2. The Interdent® gypsum is a low-porosity purified α-gypsum ($CaSO_4 \cdot ½H_2O$) used for dental purposes.

Finally, an aluminium alloy used for the production of lightweight aluminium foams Alporas® was studied. The material consists of an aluminium intermixed with 1.5 wt.% of Ca and 1.6 wt.% TiH_2. The microstructures of the selected materials are shown in Fig. 1. Dark areas in the figure can be attributed to the low density components or microporosity in the matrix, whereas lighter areas belong to individual microstructural components mentioned previously. The images show on the heterogeneity of the samples in the tested RVEs whose dimensions are ~100–200 μm.

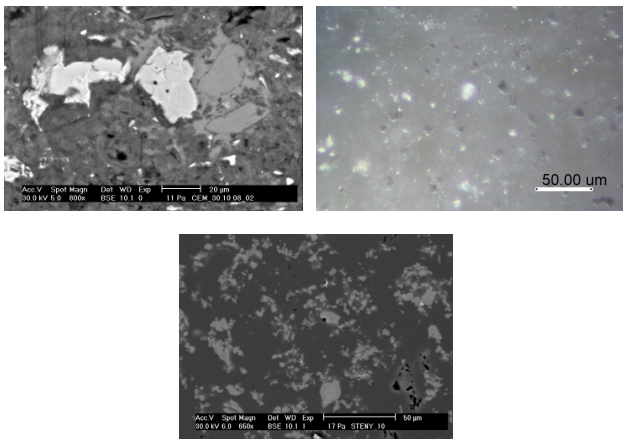

Fig. 1. **Microstructures of cement paste (top left), dental gypsum (top right) and aluminium alloy (bottom)**

5. Results

For cement paste, the microstructural RVE size consisting all the relevant material phases in a representative content is ~200 μm. Grid indentation consisting of approximately 20×20=400 indents with 10 μm spacing was performed. The indents were prescribed as load controlled (to maximum force 2 mN). Final indentation depths arrived at 200−300 nm. Frequency plots of elastic moduli (evaluated with Oliver−Pharr method[12]) were analyzed by statistical deconvolution[6]. Five distinct phases were found as shown in Fig. 2. The peaks were linked with chemically distinct phases denoted as: A=low stiffness phase, B=low density C-S-H, C=high density C-S-H, D=$Ca(OH)_2$, E=clinker. In this case, the notation of mechanically distinct phases matches well with the cement chemistry. Tab. I shows numerical results of the deconvolution and also results from the Mori-Tanaka homogenization.

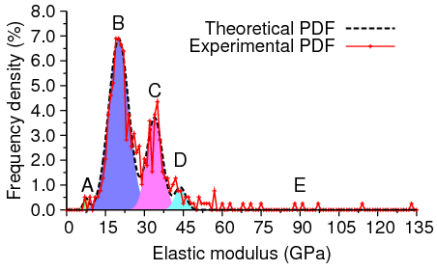

Fig. 2. **Probability density functions of elastic moduli and deconvolution on cement samples**

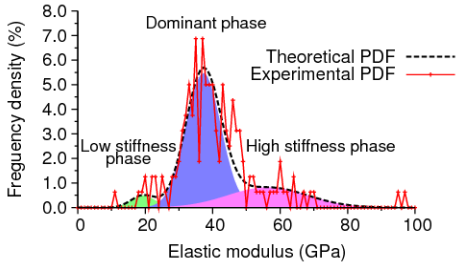

Fig. 3. **Probability density functions of elastic moduli and deconvolution on gypsum samples**

Table I
Data received from statistical deconvolution and homogenized values on cement paste

Phase	*E* [GPa] (mean value)	Poisson's ratio [-]	Volume fraction
Low stiffness (A)	7.45	0.2	0.0105
Low density C-S-H (B)	20.09	0.2	0.6317
High density C-S-H (C)	33.93	0.2	0.2634
$Ca(OH)_2$ (D)	43.88	0.3	0.0461
Clinker (E)	130*	0.3	0.0483
M-T homogenized value	25.3308	0.2067	1.0

*Note: The clinker E-value was adjusted according to ref.[10]

Similar microstructural RVE ~200 µm could be recognized on gypsum samples. Gypsum is characterized with the directionless crystalline microstructure. Indentation matrices containing 15×12=180 indents with 15 µm spacing covered the tested RVE. The same loading as in case of cement was used. Three peaks (low stiffness, dominant and high stiffness phases) were identified in frequency plots of elastic moduli as depicted in Fig. 3. Tab. II shows deconvolution results and Mori-Tanaka homogenization.

Two mechanically distinct phases were found by the statistical deconvolution on Al-alloy sample (Fig. 4). Loading to maximum force 1 mN (final depth ~200 nm) was used. Results from 200 indents (two locations 10×10 indents) with 10 µm spacing were evaluated. The RVE size is ~100 µm in this case. According to the SEM-EDX studies, the dominant phase was denoted as Al-rich zone, whereas the lower stiffness phase as Ca/Ti-rich area. Again, Tab. III shows numerical results and homogenized Mori-Tanaka effective elastic modulus.

Table II
Data received from statistical deconvolution and homogenized values on gypsum

Phase	E (GPa) (mean value)	Poisson's ratio (-)	Volume fraction
Low stiffness	19.357	0.2	0.04375
Dominant	37.234	0.2	0.71250
High stiffness	56.277	0.2	0.24375
M-T homog.	40.000	0.2	1.0

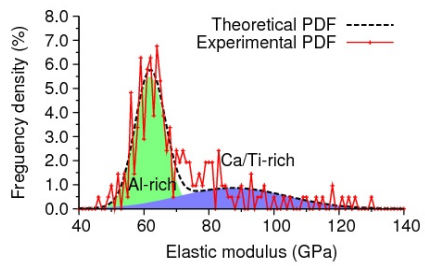

Fig. 4. **Probability density functions of elastic moduli and deconvolution on Al-alloy**

Table III
Data received from statistical deconvolution and homogenized values on Al-alloy

Phase	*E* [GPa] (mean value)	Poisson's ratio [-]	Volume fraction
Al-rich zone	61.882	0.35	0.63768
Ca/Ti-rich zone	87.395	0.35	0.36232
M-T homog.	70.083	0.35	1.0

Results from FFT-based homogenization were received in the form of plane strain stiffness matrices. Generally, anisotropy can be obtained in the numerical compu-

tation. However, it was found that for our materials the anizotropy is very low and related stiffnesses are close to isotropic ones as illustrated for cement in the following equations, in which stiffness matrices computed from analytical solution (Eq. (*7*)) and numerical solution (Eq. (*8*)) are presented.

$$\mathbf{L}_{\mathbf{eff}}^{\mathbf{A}} = \begin{bmatrix} 28.145 & 7.036 & 0 \\ 7.036 & 28.145 & 0 \\ 0 & 0 & 21.109 \end{bmatrix} \tag{7}$$

$$\mathbf{L}_{\mathbf{eff}}^{\mathbf{FFT}} = \begin{bmatrix} 26.177 & 6.778 & 0.068 \\ 6.778 & 26.224 & 0.014 \\ 0.068 & 0.014 & 19.818 \end{bmatrix} \tag{8}$$

Note that stiffness matrices in Eq. 7 and 8 are in Mandel's notation. It can be seen that off-axis terms are close to zero which shows on the mentioned very low anizotropy. The difference between the solutions can be characterized with the following matrix error norm:

$$\delta = \sqrt{\frac{\left(\mathbf{L}_{\mathbf{eff}}^{\mathbf{FFT}} - \mathbf{L}_{\mathbf{eff}}^{\mathbf{A}}\right) : \left(\mathbf{L}_{\mathbf{eff}}^{\mathbf{FFT}} - \mathbf{L}_{\mathbf{eff}}^{\mathbf{A}}\right)}{\left(\mathbf{L}_{\mathbf{eff}}^{\mathbf{FFT}} : \mathbf{L}_{\mathbf{eff}}^{\mathbf{FFT}}\right)}} \tag{9}$$

Respective error norms for cement, gypsum and aluminium alloy are as follows:

$${}^{cem}\delta = 0.071045 \ , \ {}^{gyps}\delta = 0.075138 \ , \ {}^{Al}\delta = 0.0393058 .$$

6. Discussion

The analytically computed effective RVE stiffnesses are in good agreement with those obtained from numerical FFT-based solution. The error is 3.9−7.5 % for the studied materials. Also, the estimated overall elastic moduli are in good agreement with those experimentally measured on larger-scale composite samples for cement[10,13,14], gypsum[15] and Alporas[16].

It was also proved that both simple analytical and numerical FFT-based method give comparable results in our case which is primarily due to the close-to-isotropic nature of the tested materials within the specified RVE.

7. Conclusions

It was shown in this paper that micromechanical homogenization methods can be efficiently used for obtaining effective elastic properties on heterogeneous structural materials. Local mechanical properties were found with the aid of statistical nanoindentation and deconvolution methods that give access to both phase properties as well as their volume fractions. Effective properties of RVEs (100−200 μm) of the three tested materials (cement paste, gypsum and aluminium alloy) were successfully determined with an analytical Mori-Tanaka scheme and numerical FFT-based method. The performance of both approaches was in good agreement for the tested materials as validated against independent macroscopic experimental results. Derived stiffness matrices can be further utilized in standard FEM software, for the development of a multiscale model or for the optimization of the material.

Support the Czech Science Foundation (GAČR P103/09/1748 and P105/12/0824) is gratefully acknowledged.

REFERENCES

1. Zaoui A.: J. Eng. Mech. *128*, 808 (2002).
2. Eshelby J. D.: Proc. Royal Soc. A *241*, 376 (1957).
3. Mori T., Tanaka K.: Acta Metal *21*, 571 (1973).
4. Constantinides G. et al.: Mater. Sci. Eng. A *430*, 189 (2006).
5. Němeček J., Lukeš J.: Chem Listy *104*, s279 (2010).
6. Němeček J., Šmilauer V., Kopecký L.: Cem. Concr. Compos. *33*, 163 (2011).
7. Sorelli L. et al.: Cem. Concr. Res. *38*, 1447 (2008).
8. Michel J.C., Moulinec H., Suquet P.: J. Numer. Met. Eng. *52*, 139 (2001).
9. J. Zeman, J. Vondřejc, J. Novák, I. Marek: J. Comp. Phys. *229*, 8065 (2010).
10. Němeček J.: Mater. Charact. *60*, 1028 (2009).
11. Tesárek P., Němeček J.: Chem Listy *105*, s852 (2011).
12. Oliver W. C., Pharr G. M.: J. Mater. Res. *7*, 1564 (1992).
13. Constantinides G., Ulm F.-J.: J. Mech. Phys. Solids *55*, 64 (2007).
14. Hughes J. J., Trtik P.: Mater. Charact. *53*, 223 (2004)
15. http://ciks.cbt.nist.gov/garbocz/monograph
16. Jeon I. et. al.: Mech. Mater. *41*, 60 (2009).

J. Němeček, V. Králík, and J. Vondřejc *(Czech Technical University in Prague, Faculty of Civil Engineering):* **Up-scaling Microlevel Elastic Properties of Heterogeneous Structural Materials**

The paper shows micromechanical methods used for finding effective elastic properties of selected structural composites (cement, gypsum, aluminium alloy). Phase properties of the composites are received with the use of grid nanoindentation and statistical deconvolution. Elastic moduli for representative volume elements with ~100−200 μm dimensions were assessed with analytical Mori-Tanaka and numerical FFT-based methods with good agreement.

ON THE USE OF DIFFERENT INSTRUMENTED INDENTATION PROCEDURES FOR HVOF SPRAYED COATINGS

JIŘÍ NOHAVA[a], ŠÁRKA HOUDKOVÁ[b], and PETR HAUŠILD[c]

[a] CSM Instruments, Rue de la Gare 4, 2034 Peseux, Switzerland, [b] Research and Testing Institute Plzeň, Tylova 46, 301 00 Plzeň, [c] Czech Technical University in Prague, Faculty of Nuclear Sciences and Physical Engineering, Department of Materials, Trojanova 13, 120 00 Prague, Czech Republic
jiri.nohava@csm-instruments.com

Keywords: nanoindentation, grid indentation, HVOF

1. Introduction

Though the instrumented indentation itself is relatively well-known, it is not yet widely used in the thermal spray community. In the research of thermal spray coatings[1] (TSC), the instrumented indentation has however a great advantage of testing the material at various scales: at the 'nano' or 'micro' levels, where either the individual coatings constituents or the whole blocks of the coating are tested[2,3]. However, as with many novel methods one must be very careful when choosing the testing conditions as errors could easily be introduced in the measurements.

This paper intends to compare two indentation methods for determining the mechanical properties of individual phases in HVOF sprayed cermets: grid indentation and isolated indentation. The grid indentation is based on performing a large matrix of indentations and statistical evaluation of the results[4,5]. The aim of the isolated indentation, on the other hand, is to precisely position the indent so that only properties near the selected area are measured. This paper shows the results on three types of HVOF cermets and discusses the advantages and suitability of each method for this particular type of material.

2. Experimental details

Three types of HVOF sprayed coatings were selected for the experiments: WC-17%Co, Cr_3C_2-25%NiCr and (Ti,Mo)(C,N)-39%NiCo (all wt.%). For simplicity, the samples were labeled as WCCo, CrCNiCr and TiMoCN. The coatings were sprayed using optimized parameters published elsewhere[6]. An example of typical matrix-carbide structure of these coatings is shown in Fig. 1.

The WCCo coatings microstructure consisted of WC grains with size of a few micrometers and smaller. The dimensions of the carbide grains in the CrCNiCr coating were larger than in the WCCo coating.

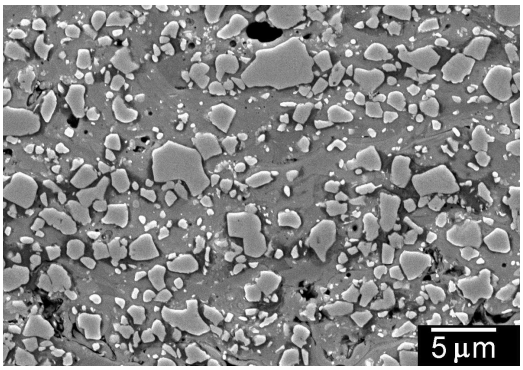

Fig. 1. **SEM images of the microstructure of the WCCo coating**

The dimensions of the hard phase grains in the TiMoCN coating were significantly smaller than those of the other coatings. The core-rim structure of the hard particles is composed of hard TiC centre core surrounded by Mo rich rim. The microstructure and mechanical properties of the (Ti,Mo)(C,N)-NiCo coating are described in more detail in Refs.[7,8].

2.1. Methods

The method of instrumented indentation[9,10] was used in all cases except for micro hardness Vickers measurements where conventional method was used. The isolated nanoindentation consisted in performing 2 mN indentations on each phase separately. At least 10 indentations were performed in several regions on each sample.

The grid indentation method is based on performing several hundreds of indentations and their subsequent statistical evaluation. The grid indentation was performed with the same indentation parameters as the isolated indentation (F_{max} 2 mN). A square matrix of 20×20 indentations spaced by 5 µm was performed in two randomly selected regions on each sample and the results were statistically evaluated using bimodal Gaussian distribution (*1*) where H_{IT} is hardness, p is mixing parameter and μ_1, σ_1, μ_2, σ_2 are the parameters of distribution.

$$f = \frac{1-p}{\sqrt{2\pi}\sigma_1}\exp\left[-\frac{(H_{IT}-\mu_1)^2}{2\sigma_1^2}\right] + \frac{p}{\sqrt{2\pi}\sigma_2}\exp\left[-\frac{(H_{IT}-\mu_2)^2}{2\sigma_2^2}\right] \qquad (1)$$

As it will be shown further, several aspects of the grid indentation on this particular type of material caused that also trimodal Gaussian distribution was considered for the statistical analysis of the results. This distribution was used in form of Eq. (*2*):

$$f = \sum_{i=1}^{3} \frac{p_i}{\sqrt{2\pi}\sigma_i} \exp\left[-\frac{(H_{IT} - \mu_i)^2}{2\sigma_i^2} \right] \cdots \sum_{i=1}^{3} p_i = 1 \qquad (2)$$

where μ_1, σ_1, μ_2, σ_2, μ_3, σ_3 are parameters of each distribution corresponding to either hardness or elastic modulus.

Both isolated and grid indentation was done using Table Top Nano Indentation Tester (CSM Instruments, Peseux, Switzerland) with diamond Berkovich indenter. Further, microindentation experiments were performed on each sample with 5 N load using Micro Indentation Tester (CSM Instruments, Peseux, Switzerland) with diamond Vickers indenter. Conventional microhardness measurements were performed on LECO DM-400A hardness tester using load of 300 g. Ten measurements were performed in the center line of each coating. The scanning electron microscopy (SEM) images were acquired using JEOL JSM 5510LV and 6490LV scanning electron microscopes.

3. Results

3.1. Isolated indentation

During the isolated indentation the indentations were placed separately in the matrix and the carbides. It was relatively straightforward to locate and position the indentations in the carbides and matrix on samples WCCo and CrCNiCr, however it was almost impossible on the TiMoCN coating. Although the boundaries between the (Ti,Mo)(C,N) and NiCo phases were clearly visible in SEM images, they did not yield sufficient contrast in optical microscope.

The results of isolated nanoindentation (2 mN) and non-selective microindentation (5 N) results on all three tested samples are compared in Table I. The values of hardness and elastic modulus show good agreement with those of bulk material[11] which confirms the utility of low load nanoindentation for measurements of mechanical properties of individual phases in HVOF coatings.

3.2. Grid indentation

The results of the grid indentation in form of elastic modulus histogram for the three tested samples are shown in Fig. 2. The bar graphs represent the measured data, the dashed lines represent each of the distributions as defined by Eq. (*1*) and the solid line is the sum of two distributions. The parameters of the individual distributions correspond to the average and standard deviation of E_{IT} values of each of the phase present in the coating.

The WCCo and CrCNiCr coatings contained two phases with distinct mechanical properties (see Table I) while the TiMoCN coating contained two phases whose mechanical properties were quite close. Expected two-peak behavior was found only for the E_{IT} histogram of the CrCNiCr coating (Fig. 2b) where the parameters of the two distributions corresponded very well to the isolated indentation results. In the case of the two other coatings, the parameters of the bimodal fit did not reflect exactly the properties of the individual phases as obtained by isolated indentation.

It was mainly the parameter of the second distribution (μ_2) that did not correspond to the results of isolated indentations in carbides. Similar difference was found also for H_{IT} histograms and the isolated indentation values.

Closer observation of the E_{IT} histograms revealed that their shape shall be better described as trimodal rather than bimodal. Considering Fig. 2a one can relatively clearly see three peaks instead of two peaks positioned at ~290 GPa and ~538 GPa, which would correspond to the carbide and metallic matrix values. The histogram therefore seems to reflect not a bimodal Gaussian distribution (Eq. (*1*)) but rather a trimodal Gaussian distribution. Indeed, Fig. 3 shows trimodal Gaussian fit for the E_{IT} histograms of all tested coatings. The third distribution corresponds to indentations done on the carbide-matrix boundary which significantly complicated the statistical analysis.

Table I
Isolated indentation results for all three tested coatings. H_{IT} is indentation hardness, E_{IT} is indentation modulus, h_m is the maximum indentation depth, HV_{IT} is Vickers hardness recalculated from the H_{IT} and HV_{03} is conventional Vickers microhardness measured with 300 g load

Coating	Phase	H_{IT} [GPa]	E_{IT} [GPa]	h_m [nm]	HV_{IT} 5N	HV_{03}
WCCo	Carbides	33.3 ± 2.7	538 ± 25	57 ± 1	1279	1335
	Matrix	16.7 ± 2.2	290 ± 27	79 ± 5		
CrCNiCr	Carbides	26.0 ± 4.0	337 ± 49	68 ± 5	777	700
	Matrix	11.2 ± 3.2	226 ± 44	96 ± 10		
TiMoCN	(Ti,Mo)(CN)-rich	13.1 ± 2.2	208 ± 32	90 ± 7	782	803
	NiCo-rich	12.2 ± 1.0	214 ± 13	92 ± 4		

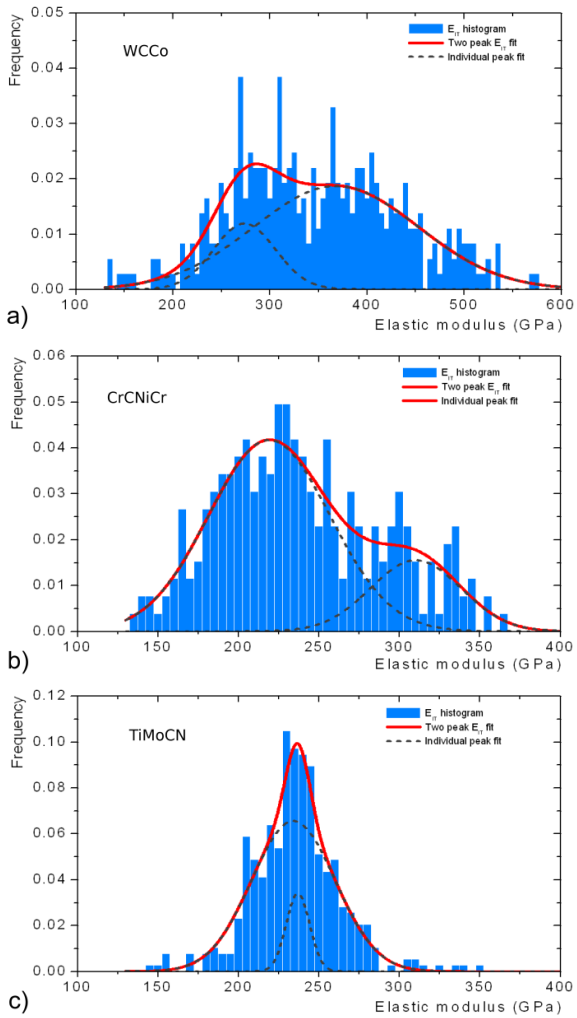

Fig. 2. **Elastic modulus histogram for the WCCo coating (a), CrCNiCr (b) and TiMoCN (c) coatings**

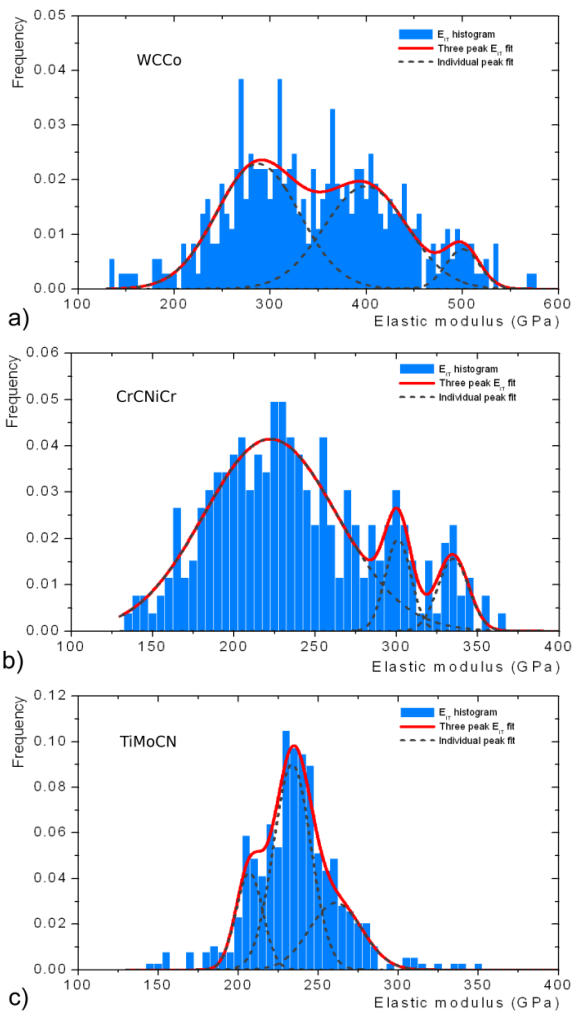

Fig. 3. **Trimodal Gaussian distribution of the E_{IT} histograms for (a) WCCo, (b) CrCNiCr and (c) TiMoCN coatings**

4. Discussion

4.1. Isolated nanoindentation and microindentation

The carbides and metallic matrix in the WCCo and CrCNiCr coatings were easily distinguishable under optical microscope attached to the indentation system. The 2 mN indentations were shallow enough (maximum penetration between ~60 nm and ~130 nm) so that an indentation done on one phase was not significantly influenced by the neighboring phase. In the case of the WCCo and CrCNiCr coatings, the properties of carbides and metallic matrix were obtained while in the case of the TiMoCN coating the properties of TiMoCN-rich and NiCo-rich phases were measured. Very similar results of $\boldsymbol{H_{IT}}$ and $\boldsymbol{E_{IT}}$ from isolated indentation of the (Ti,Mo)(C,N)–rich and NiCo-rich phases pointed out that the visual aspect is not always sufficient for distinguishing between individual phases. To properly characterize the core-rim structure the indentation experiments should be performed on a lightly etched sample where its structure would be revealed.

The high load micro indentation (5 N) was aimed on characterizing the material as a whole, including pores, carbide-matrix interfaces and boundaries, etc[12]. The values of instrumented microhardness and conventional microhardness for 5 N and 3 N loads showed very good agreement. Such agreement between the conventional and instrumented indentation is particularly important as some researchers questioned the reliability of instrumented indentation results.

4.2. Comparison of isolated and grid indentation

As showed in Fig. 2, only the grid indentation results obtained on the CrCNiCr coating showed relatively good agreement with the elastic modulus values obtained via isolated indentation. In other cases, the hardness and/or elastic modulus values obtained from statistical evaluation

of grid indentation results differed considerably from the isolated indentation values. Although the use of a bimodal distribution was expected, the trimodal distribution yielded results in better agreement with the isolated indentation values. The μ_2 parameter, representing the peak between the μ_1 and μ_3 peaks, reflected the indentations done on the carbide-matrix boundary which significantly complicated the statistical analysis. Obviously, the amount of indentations near the carbide-matrix boundary in the grid indentation was not negligible and had to be taken into account during the statistical analysis of the results.

The trimodal Gaussian fit also revealed the existence of hard phase in the TiMoCN coating with hardness of 18.7 GPa (Fig. 4) and elastic modulus of 261 GPa (see Table II). This phase was not detected when performing the isolated indentations and it very likely corresponded to the (Ti,Mo)(C,N) particles, whose hardness is expected to be higher than that of the NiCo matrix.

5. Conclusions

This paper presents the results of two methods of instrumented indentation for determination of mechanical properties of thermal spray coatings. The isolated indentation method yielded very good results with relatively low standard deviation on all three types of tested coatings. The statistical evaluation of the grid indentation was somewhat complicated due to indentations on the carbide-matrix interface. Since the number of such indentations was not negligible, the use of trimodal Gaussian distribution was necessary to extract the properties of individual phases. These properties obtained by the trimodal Gaussian fit were in very good agreement with those obtained by isolated indentation method. The grid indentation also allowed measurement of properties of phases that were difficult to locate under optical microscope.

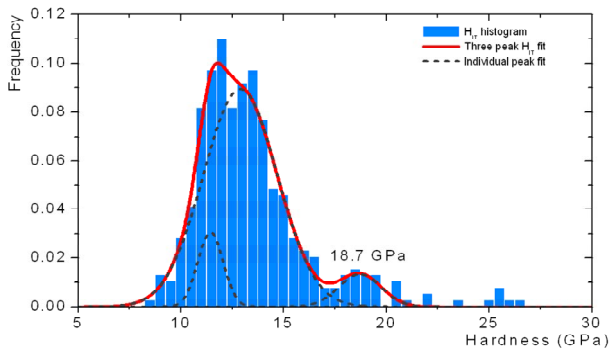

Fig. 4. **Trimodal Gaussian distribution of the H_{IT} histograms for the TiMoCN coatings showing the peak at 18.7 GPa**

Table II
Trimodal Gaussian fit of the grid indentation data compared with isolated indentation results. The standard deviation was omitted for the reasons of clarity

E_{IT} [GPa]	Trimodal			Isolated indentation	
	Soft	Intermediate	Hard	Soft	Hard
WCCo	287	399	500	290	538
CrCNiCr	222	301	335	226	337
TiMoCN	204	234	261	214	208

This work was supported by the SGS10/300/OHK4/3T/14 and VZ/MSM4771868401 projects.

REFERENCES

1. Herman H.: Sci. Am. *259*, 112 (1988).
2. Margadant N., Neuenschwander J., Stauss S., Kaps H., Kulkarni A., Matejicek J., Roessler G.: Surf. Coat. Technol. *200*, 2805 (2006).
3. Racek O., Berndt C. C.: Surf. Coat. Technol. *202*, 362 (2007).
4. Randall N. X., Vandamme M., Ulm F.-J.: Mater. Res. *24*, 679 (2009).
5. Constantinides G., Chandran K. S. R., Ulm F.-J., Van Vliet K. J.: Mater. Sci. Eng. A *430*, 189 (2006).
6. Houdková Š., Zahálka F., Kašparová M., Berger L.-M.: Conf. Proc. ITSC 2008, Maastricht (NL), 1485 (2008).
7. Berger L.-M., Woydt M., Zimmermann S., Keller H., Schwier G., Enžl R., Thiele S.: Conf. Proc. ITSC 2004, Osaka (JP), 10 (2004).
8. Berger L.-M., Zimmermann S., Keller H., Schwier G., Thiele S., Nebelung M., Enžl R.: Conf. Proc. ITSC 2003, 793 (2003).
9. Fischer-Cripps A. C.: Springer, New York 2004.
10. Oliver W. C., Pharr G. M.: J. Mater. Res. *19*, 3 (2004).
11. Lengauer W.: *Handbook of Ceramic Hard Materials*, Wiley, 202 (2000).
12. Nohava J., Bonferroni B., Bolelli G., Lusvarghi L.: Surf. Coat. Technol. *205*, 1127 (2010).

J. Nohava[a], Š. Houdková[b], and P. Haušild[c] *([a] CSM Instruments, Peseux, Switzerland; [b] Research and Testing Institute Plzeň, Czech Republic; [c] Czech Technical University in Prague, Faculty of Nuclear Sciences and Physical Engineering, Department of Materials, Praha, Czech Republic):* **On the Use of Different Instrumented Indentation Procedures for HVOF Sprayed Coatings**

This work compares the isolated nanoindentation with grid indentation on three HVOF coatings. The bimodal and trimodal Gaussian fits are compared with the isolated indentation results and the reasons for the use of trimodal fit are given. The results are completed by comparison of conventional and instrumented micro indentation results.

VISCOELASTIC PROPERTIES OF PORCINE APOPHYSEAL JOINT

MARTIN OTÁHAL[a], JOSEF ŠEPITKA[b], JAROSLAV LUKEŠ[b], and MIROSLAV SOCHOR[b]

[a] *Charles University in Prague, Faculty of Physical Education and Sport, Laboratory of Biomechanics of Extreme Loads, José Martího 31 Prague 190 00,* [b] *Czech Technical University in Prague, Faculty of Mechanical Engineering, Dep. of Mechanics, Biomechanics and Mechatronics, Technicka 4, 166 07 Prague , Czech Republic*
martinotahal@ftvs.cuni.cz

Keywords: spine, apophyseal joint, cartilage, nanoindentation, DMA

1. Introduction

Problem of low back pain is still one of the main problems in a spinal biomechanics. This study is focused on viscoelastic properties of apophyseal joint. Mechanical properties and a shape of apophyseal joints define a small interspaces needed for preserving the principles of the preferred movements, which is defined by the shape of the vertebra and by the viscoelastic behavior of the passive elements of intervertebral joint ligaments, the intervertebral disc, etc. and the tuned movements of intervertebral joint (IVJ) (movements defined by the elements of the active control-muscle system and central nervous system)[1].

Apophyseal joints (Fig. 1) are composed of two neighboring articular processes enclosed in the joint capsule. Facets of both articular processes are covered by thin cartilage layers like in synovial joint[2].

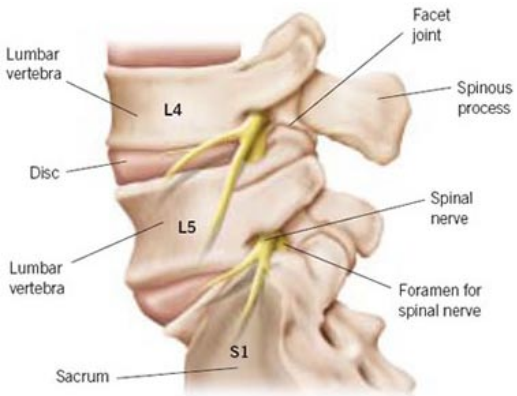

Fig. 1. **Spinal motion segments.** Apophyseal (facet) joints are small joints on each side at the back of the spine which allow movement between adjacent vertebrae while maintaining a spinal stability

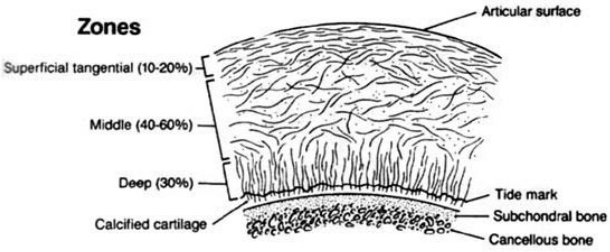

Fig. 2. **Structure of articular cartilage, orientation of collagen fibers.** Arrows show testing directions of the samples

An articulating cartilage is very important part of apophyseal joint from the rheological point of view. Dynamic nanoindentation is one of the possible methods to obtain viscoelastic properties of articular cartilage. Porcine vertebra was used as a biological model of human vertebra in this study.

2. Materials and methods

A porcine apophyseal joint of lumbar spine L4-L5 was used in our study. A specimen of cartilage was cut from fresh porcine vertebra, dissected from 1.5 year old animals. Two specimens were sliced and polished from a single joint. Thus, two surfaces were prepared for nanoindentation in normal and lateral direction to the joint facets. Specimens were submerged into a saline solution immediately after the preparation. Dynamic testing was also carried out within physiological solution.

Each joint was tested in two directions at different locations. Two locations were indented in normal direction and an edge of the cartilage, a central layer of the cartilage and a transition zone between the cartilage and subchondral bone were indented in lateral direction (Fig. 2).

NanoDMA load controlled experiment was performed with Hysitron TriboIndenter™ system with Berkovich diamond tip at the temperature 23.9 °C. Harmonic loading $P_0 = \sin(\omega t)$ with dynamic load amplitude $P_0 = 0.5$ μN was specified for the harmonic frequency range 30–200 Hz. During nanoDMA experiment, static load was applied at maximum force $P_{max} = 200$ μN (ref.[3]). Following amplitude of displacement oscillation X_0, and Φ the phase shift between force and displacement signal are recorded by the nanoindentation system. The machine compliance value C_i and the stiffness value K_i were determined during air indentation calibration. The procedure was adopted from Asif et al. (1999)[4].

The reduced storage modulus (E_r'), the reduce loss modulus (E_r'') and $\tan\delta = E_r''/E_r'$ dependent on compliance and stiffness of the sample are given by

$$E'_r = \frac{K_s\sqrt{\pi}}{2\sqrt{A}}, \quad E''_r = \frac{\omega C_s\sqrt{\pi}}{2\sqrt{A}} \text{ and } \quad \tan\delta = \frac{C_s\omega}{K_s}$$

where A_c is the contact area based on tip area function related to the contact depth at quasistatic loading[5]

The storage modulus and the loss modulus are related to the complex modulus $E_r^* = E_r' + iE_r''$ and indicate the ability of the material to return energy (E_r') and dissipate energy (E_r''). The ratio of the loss modulus to the storage modulus (i.e., tan δ) reflects the viscoelastic behavior of a material, which is called damping. It is a material parameter independent of a tip-sample contact area[6].

3. Results

Dynamic mechanical characteristics were obtained for the specimens in a range of frequencies 30–200 Hz. Firstly; two locations in normal direction were analyzed. Secondly; the edge of the cartilage, central layer of the cartilage and transition area between the cartilage and subchondral bone were analyzed in lateral direction.

Fig. 3 shows dependence of tan δ on the frequency for both tested directions. There are two noticeable different trends of tan δ. The cartilage analyzed in normal direction shows higher damping capability between 30 and 100 Hz than the cartilage analyzed in lateral direction. There is an intersection of two trends in tan δ at about 100 Hz. There is increasing trend of curves of the edge and middle layer area beyond 100 Hz. Transition area between the cartilage and subchondral bone has decreasing trend from 100 Hz the same as samples tested in normal directions.

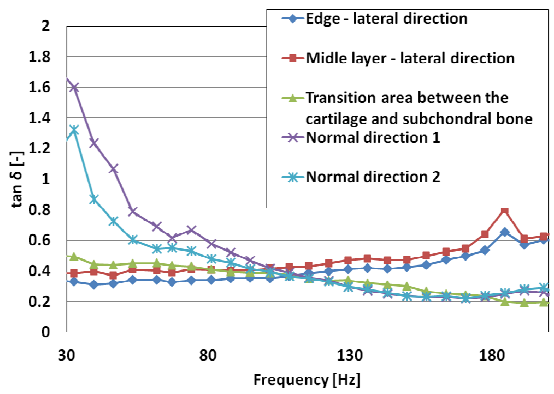

Fig. 3. **Tan δ *vs.* frequency from nanoDMA**

4. Discussion and conclusion

The results show differences of dynamic characteristics for different directions of testing on apophyseal joint. In other words, cartilage has increased ability to damp the dynamic load in normal direction from 30 to 100 Hz contrary to lateral direction. However, damping capabilities decrease within loading rates represented by frequency range. These finding are in an agreement with physiologic behavior of joints in general.

More likely, micromechanical properties reflect inner microstructure of a local region of the cartilage. Structural differences from lateral and normal point of view are clearly seen on Fig. 2. Therefore, mechanical properties vary as well. Nevertheless, structural diversity between the edge and the middle area are not that significant, therefore, mechanical properties follow the same trend. Interestingly, structurally different area close to subchondral bone showed mechanical differences only beyond 100 Hz. Hypothetically, important architectural element, highly oriented collagen fibers are employed when the frequency overcome 100 Hz.

This research was supported by Ministry of Education project: Transdisciplinary research in Biomedical Engineering II. No. MSM 6840770012 and TAČR project: No. TA01010860.

REFERENCES

1. Otahal M., Holub O., Kronek J., Sochor M., Otahal S.: J. Biomech. *41- S1*, 354 – S354 (2008).
2. Adams M., Bogduk N., Burton K., Dolan P.: *The biomechanics of back pain*. Elsevier, Oxford 2006.
3. Sepitka J., Otahal M., Lukes J.: Comput Method Biomech. *14*, 265 (2011).
4. Asif S. A. S., Wahl K. J., Colton R. J.: Rev. Sci. Instrum. *70*, 2408 (1999).
5. Oliver W. C., Pharr G. M.: J. Mater. Res. *7*, 1564 (1992).
6. Menard K. P: *Dynamic mechanical analysis*. Taylor & Francis Group, Boca Raton 2008.

M. Otáhal[a], J. Šepitka[b], J. Lukeš[b], and M. Sochor[b] *([a] Laboratory of Biomechanics of Extreme Loads, Faculty of Physical Education and Sport, Charles University in Prague, [b] Czech Technical University in Prague, Faculty of Mechanical Engineering, Dep. of Mechanics, Biomechanics and Mechatronics, Prague, Czech Republic):* **Viscoelastic Properties of Porcine Apophyseal Joint**

This study is focused on viscoelastic properties of an apophyseal joint. Dynamic nanoindentation was used for a characterization of viscoelastic properties of an articular cartilage. Micromechanical properties reflect inner microstructure of local regions of the cartilage. The results are discussed with respect to the cartilage microstructure in this paper.

IRRADIATED POLYPROPYLENE STUDIED BY MICROHARDNESS AND WAXS

MARTIN OVSIK[a], DAVID MANAS[a], MIROSLAV MANAS[a], MICHAL STANEK[a], MARTINA HRIBOVA[a], KAREL KOCMAN[a], DAVID SAMEK[a], and MARTIN MANAS[b]

[a] *Tomas Bata University in Zlin, Faculty of Technology, Department of Production Engineering, TGM 5555, 760 01 Zlin, Czech Republic,* [b] *MITAS a. s., Švehlova 1900, 106 25 Prague 10, Czech Republic*
dmanas@ft.utb.cz

Keywords: microhardness, irradiation crosslinking, polypropylene, X-ray diffraction

1. Introduction

Isotactic polypropylene is a commodity polymer of a semi-crystalline structure which is very complex and depends strongly on thermal history and processing conditions. Isotactic polypropylene can crystallize into 3 phases: alpha phase is the most stable and the most known. The crystals are monoclinic. Beta phase is metastable and the crystals are hexagonal. β-phase is mainly found in block PP copolymers and can be generated by addition of specific nucleating agents. This phase was discovered by Padden and Keith in 1953 and can be improved by crystallization between 130 and 132 °C or by orientation with high shear or through addition of specific nucleating agents. Presence of β-phase in PP homopolymer generally increase ductility in the finished parts. Maximum effect is observed at 65 % of β-phase. γ-phase – this phase is also metastable with triclinic crystals. This form is not very familiar but appears mainly in low molecular weight polypropylene by crystallization at a very high pressure and a very low cooling rate[1,2].

The irradiation cross-linking of thermoplastic materials via electron beam or cobalt 60 (gamma rays) is proceeding separately after the processing. The cross-linking level can be adjusted by the irradiation dosage and often by means of a cross-linking booster[1,2].

The main diference between β- and γ-rays is in their different abilities of penetrating the irradiated material. γ-rays have a high penetration capacity. The penetration capacity of electron rays depends on the energy of the accelerated electrons.

Due to electron accelerators the required dose can be applied within seconds, whereas several hours are required in the γ-radiation plant.

The electron accelerator operates on the principle of the Braun tube, whereby a hot cathode is heated in vacuum to such a degree that electrons are released.

Simultaneously, high voltage is generated in a pressure vessel filled with insulating gas. The released electrons are accelerated in this vessel and made to fan out by means of a magnetic field, giving rise to a radiation field. The accelerated electrons emerge via a window (Titanium foil which occludes the vacuum) and are projected onto the product.

Cobalt 60 serves as the source of radiation in the gamma radiation plant. Many of these radiation sources are arranged in a frame in such a way that the radiation field is as uniform as possible. The palleted products are conveyed trough the radiation field. The radiation dose is applied gradually, that is to say, in several stages, whereby the palleted products are conveyed around the Co – 60 radiation sources several times. This process also allows the application of different radiation doses from one product type to another. The dimensional stability, strength, chemical resistance and wear of polymers can be improved by irradiation. Irradiation cross-linking normally creates higher strength as well as reduced creep under load if the application temperature is above the glass transition temperature (T_g) and below the former melting point. Irradiation cross-linking leads to a huge improvement in resistance to most of the chemicals and it often leads to the improvement of the wear behaviour.

The thermoplastics which are used for production of various types of products have very different properties. Standard polymers which are easy obtainable with favourable price conditions belong to the main class. The disadvantage of standard polymers is limited both by mechanical and thermal properties. The group of standard polymers is the most considerable one and its share in the production of all polymers is as high as 90 %.

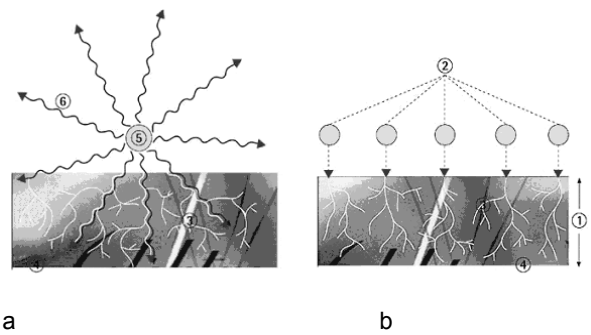

Fig. 1. **Design of Gamma rays (a) and Electron rays (b);** a) 3 – secondary electrons, 4 – irradiated material, 5 – encapsulated Co – 60 radiation source, 6 – Gamma rays; b) 1 – penetration depth of electron, 2 – primary electron, 3 – secondary electron, 4 – irradiated material

The engineering polymers are a very important group of polymers which offer much better properties in comparison to those of standard polymers. Both mechanical and thermal properties are much better than in case of standard polymers. The production of these types of polymers takes less than 1 % of all polymers.

High performance polymers have the best mechanical and thermal properties but the share in production and use of all polymers is less than 1 %.

Common PP, when exposed to the effect of the radiation cross-linking, degrades and its mechanical properties deteriorate. Using cross-linking agent TAIC (triallyl isocyanurate) produces a cross-linking reaction inside the PP structure. The utility properties of PP improve when the noncrystalline part of PP is cross-linked[3–5].

The present work deals with the influence of morphlogy on the microhardness of irradiated crosslinked polypropylene.

2. Experimental

For this experiment polypropylene PP PTS –Crealen EP-2300L1-M800; PTS Plastics Technologie Service, Germany (unfilled, iPP+TAIC, MFR – 230 °C /2.16 kg – 6 g/10 min) was used. The material already contained the special cross-linking agent TAIC – triallyl isocyanurate (5 volume %), which should enable subsequent cross-linking by ionizing β – radiation. The prepared specimens were irradiated with doses of 30, 45, 60 and 90 kGy at BGS Beta-Gamma Service GmbH & Co. KG, Germany[4–6].

The samples were made using the injection molding technology on an injection moulding machine Arburg Allrounder 420C. Processing temperature 210–240 °C, mold temperature 50 °C, injection pressure 80 MPa, injection rate 50 mm s^{-1}.

Instrumented microhardness tests were done using a Micro Combi Tester, CSM Instruments (Switzerland) according to the CSN EN ISO 6507-1. Load and unload speed was 2 N min^{-1}. After a holding time of 90 s at maximum load 1 N the specimens were unloaded. The indentation hardness H_{IT} was calculated as maximum load to the projected area of the hardness impression according to:

$$H_{IT} = \frac{F_{\max}}{A_p} \text{ with } \qquad h_c = h_{\max} - \varepsilon \frac{F_{\max}}{S} \qquad (1)$$

where h_{max} is the indentation depth at F_{max}, h_c is contact depth. In this study the Oliver and Pharr method was used calculate the initial stiffnes (S), contact depth (h_c). The specimens were glued on metallic sample holders[5–7].

Wide angle X-ray diffraction patterns were obtained using a PAN alytical X-pert Prof X-ray diffraction system (Netherlands). The CuK_α radiation was Ni-filtered. The scans (4.5 ° 2Q/min) in the reflection mode were taken in the range 5–30° 2Θ. The sample crystallinity X was calculated from the ratio of the crystal diffraction peaks and the total scattering areas[7–9].

3. Results and discussion

Fig. 2 shows typical X-ray diffraction spectrum of the non-irradiated and irradiated polypropylene. There is an apparent presence of α-phase and β-phase in the non-irradiated specimen. A gradual loss of β-phase can be seen with growing radiation dose, with its maximum loss seen at a radiation dose of 60 kGy (Fig. 2). The greatest loss of α-phase is seen at the radiation dose of 45 kGy (Fig. 2).

The results of the crystal size for non-radiated and irradiated polypropylene are shown in the Fig. 3. The values measured show some heterogeneity of the crystal sizes at individual radiation doses (225–300 Å). When applying β-radiation the structure of polypropylene undergoes a loss of the crystalline phase. It can be assumed that the size of individual crystals will correspond to the loss of crystalline phase (crystalline value X calculated lay in the range 40.8–54 %). Cross-linking occurs in the remaining noncrystalline part which has a significant influence on the micromechanical properties of the surface layer.

The greatest size of crystals was found in the case of the non-irradiated polypropylene (300 Å). On the contrary the smallest size of crystals (Fig. 3) was measured at radiation dose of 90 kGy (225 Å).

The process of irradiation causes physical and chemical changes in the structure of polypropylene. They are mainly changes of crystalline and amorphous phase. The measurement results show clearly that as the irradiation dose increases, the crystallinity reduces and the size of

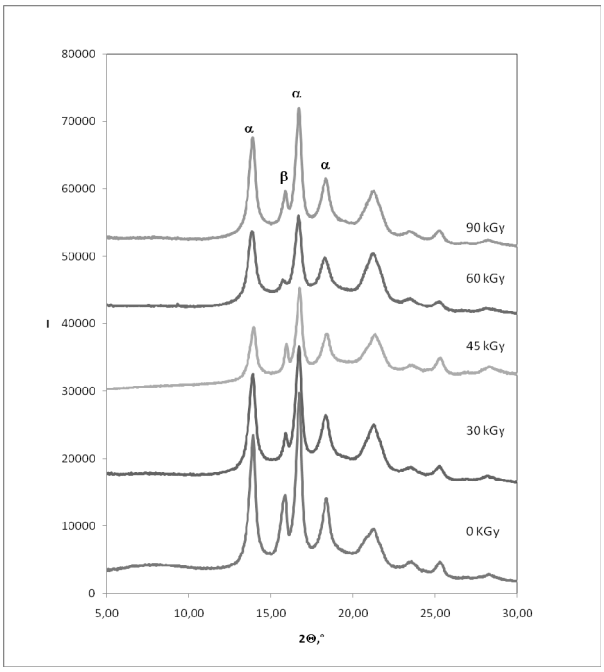

Fig. 2. **Typical X – ray diffractograms of irradiated PP**

crystals diminishes and the structure is finer. During the amorphous phase cross-linking occurs which results in creation of very solid areas as well as considerable growth of microhardness values. Higher irradiation doses do not cause greater cross-linking but rather disruption of links resulting in degradation of the irradiated material.

The values measured during the microhardness test showed that the lowest values of indentation hardness were found for the non-irradiated PP. On the contrary, the highest values of indentation hardness were obtained for PP irradiated by a dose of 45 kGy (by 75 % higher in comparison with the non-irradiated PP), as can be seen at Fig. 4.

Higher radiation dose does not influence significantly the microhardness value. An indentation hardness increase of the surface layer is caused by irradiation cross-linking of the tested specimen. A closer look at the microhardness results reveals that when the highest radiation doses are used, microhardness decreases which can be caused by radiation indusced degradation of the material.

According to the results of measurements of microhardness, it was found that the highest values of indentation modulus of elasticity were achieved at the PP irradiated with dose of 45 kGy (by 95 % higher than compared with non-irradiated PP). On the contrary, the lowest values of the indentation modulus of elasticity were found for non-irradiated PP as is seen at Fig. 5.

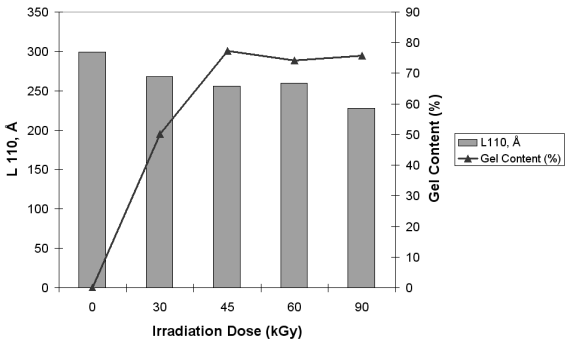

Fig. 3. **Crystals size of polypropylene *vs.* irradiation dose**

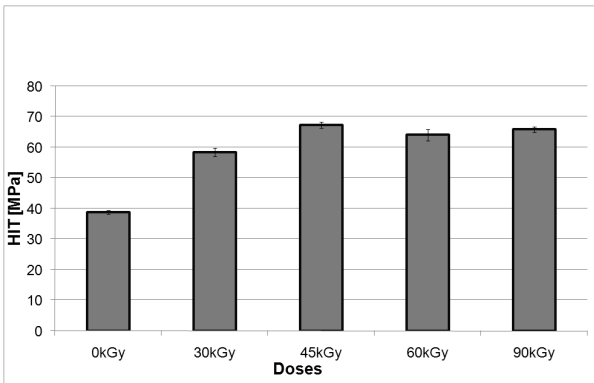

Fig. 4. **Hardness of polypropylene *vs.* irradiation dose**

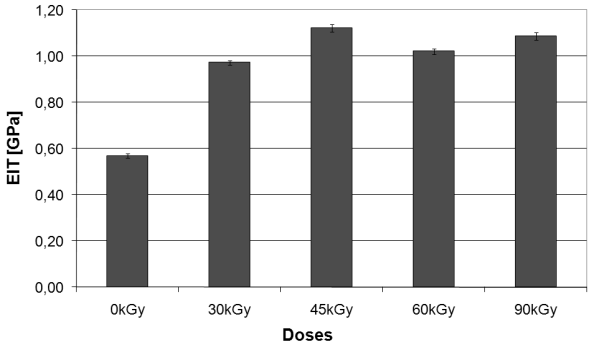

Fig. 5. **Elastic modulus of polypropylene *vs.* irradition dose**

Other important material parameters obtained during the microhardness test were elastic and plastic deformation work. The elastic deformation work W_e determines the reaction of a material to applied (multiaxial) load with reversible deformation. The plastic part of the deformation work W_{pl} defines toughness of the tested material (surface layer) and its resistance to plastic deformation (Fig. 6).

The highest values of plastic and elastic deformation work were obtained for non-irradiated PP. The lowest values of both elastic and plastic deformation work were obtained for PP irradiated with a dose of 45 kGy. Radiation of specimens caused lower values of elastic as well as plastic deformation work which is apparent in Fig. 7. This drop corresponds to the macro tests of impact strength conducted. The non-irradiated specimen did not break during impact test. However, the irradiated specimen broke during the impact test.

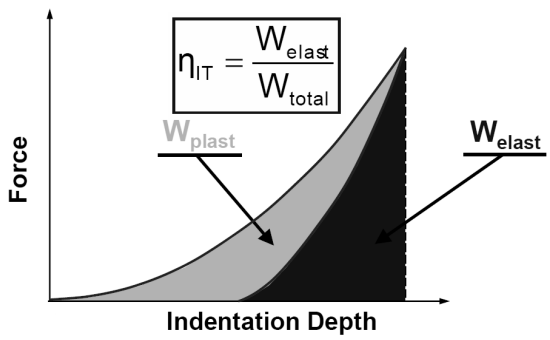

Fig. 6. **Mechanical Work of Indentation**

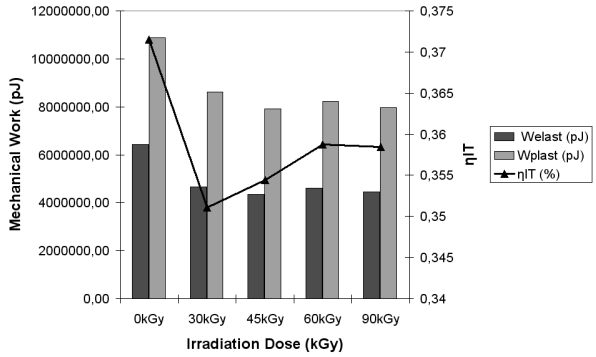

Fig. 7. **Elastic and plastic deformation work of polypropylene *vs.* irradiation dose**

Next to plastic and elastic deformation work, the coefficient of back deformation η_{IT} is especially important for the assessment of the structure of the irradiated polypropylene. The highest values were measured at non-irradiated PP. The smallest values were found at irradiation doses of 33 and 45 kGy.

4. Conclusion

Very interesting results were obtained for irradiation modified PP. When comparing the irradiated and non-irradiated PP it was apparent that the values of indentation hardness, Vickers hardness and the indentation modulus considerably increased, in some cases even by 95 % at the irradiation dose of 45 kGy. Also different depths of indentation in the surface layer of tested specimen were significantly different. It also proved the fact that higher doses of radiation do not have very positive effects on the mechanical properties, on the contrary due to degradation processes the properties deteriorate.

The opposite and deteriorated values were obtained for plastic and elastic work. In both cases the values dropped in the case of irradiated specimen. On the other hand non-irradiated PP showed high values of elastic and plastic deformation work.

This article was written with support of Ministry of Industry of Czech Republic as a part of the project called Development of the system for evaluation of hardness testing with stress on the research of new possibilities of polymer material characteristics analysis and application of the results on the market. FR-TI1/487.

REFERENCES

1. Manas D., Manas M., Stanek M., Danek M.: Arch. Mater. Sci. Eng. *32*, 69 (2008).
2. Uzuna O., Kölemena U., Çelebi S., Güçlü N.: J. Eur. Ceram. Soc. *25*, 969 (2005).
3. Stanek M., Manas M., Manas D.: *Novel Trends in Rheology III*, AIP, New York, USA, p. 75–85 (2009).
4. Oliver W. C., G. M. Pharr.: J. Mater. Res. *7*, 1564 (1992).
5. Chvatalova L., Navratilova J., Cermak R., Raab M., Obadal M.: Macromolecules *42*, 7413 (2009).
6. Stanek M., Manas D., Manas M., Suba O.: J. Mathematics Computers Simulation *5*, 422 (2011).
7. Manas D., Stanek M., Manas M., Pata V., Javorik J.: KGK, Kautsch. Gummi Kunstst. *62*, 240 (2009).
8. Manas M., Stanek M., Manas D., Danek M., Holík Z.: Chem. Listy *103*, s24 (2009).
9. Manas D., Manas M., Stanek M., Zaludek M., Sanda S., Javorik J., Pata V.: Chem. Listy *103*, s72 (2009).

M. Ovsik[a], D. Manas[a], M. Manas[a], M. Stanek[a], M. Hribova[a], K. Kocman[a], D. Samek[a], and Manas M.[b]
([a] Tomas Bata University in Zlin, Faculty of Technology, Department of Production Engineering, Zlin, [b] MITAS a. s., Prague, Czech Republic): **Irradiated Polypropylene Studied by Mircohardness and Waxs**

Hard surface layers of polymer materials, especially polypropylene, can be formed by chemical or physical process. One of the physical methods modifying the surface layer is radiation cross-linking. Radiation doses used were 0, 30, 45, 60 and 90 kGy for unfilled polypropylene with the 5 % cross-linking agent (triallyl isocyanurate). Individual radiation doses caused structural and micromechanical changes which have a significant effect on the final properties of the polypropylene tested. Small radiation doses cause changes in the surface layer which make the values of some material parameters rise. The improvement of micromechanical properties was measured by an instrumented microhardness test. X-ray diffraction was used to study the influence of the structure.

MICROSTRUCTURE AND PROPERTIES OF THE Ni-Al-B ALLOYS AFTER DIRECTIONAL SOLIDIFICATION

MARTIN POHLUDKA, JITKA MALCHARCZIKOVÁ, and MIROSLAV KURSA

VŠB – Technical University of Ostrava, 17. listopadu 15/2172, 708 33 Ostrava Poruba, Czech Republic
martin.pohludka@vsb.cz

Keywords: Ni-Al-B alloys, microstructure, porosity, microhardness

1. Introduction

Ni_3Al intermetallic compound exhibits anomalous deformation behaviour due to the unique structure of $L1_2$. This behaviour is characterised by an increase of deformation stress with temperature up to 800 °C. Then the stress decreases. Therefore Ni_3Al based alloys are used in high temperature applications such as turbine blades[1].

Brittleness of polycrystalline Ni_3Al at room temperature inhibited its usage in industry in past. The brittleness is caused by air moisture which weakens the grain boundaries by accumulation of atomic hydrogen. The brittleness can be reduced by boron alloying of these alloys. Boron protects from a hydrogen placement along grain boundaries and it cohesively strengthens them. Ni-24Al-0.24B alloy (at. %) achieves the best mechanical properties[2].

2. Experiment

Ni-24Al, Ni-24Al-0.1B and Ni-24Al-0.24B alloys (at.%) were prepared by melting in a vacuum induction furnace. After grinding of surface oxide layer, the cast of every alloy was directionally solidified in the super Kanthal resistance furnace used the Bridgman's method at the temperature of 1550 °C and at the rate of 50 mm h^{-1}. The transversal sections were cut from the as-cast (C) and the as-directionally solidified (DS) samples for documentation of microstructure and for evaluation of porosity and microhardness.

3. Results

3.1. Microstructure

Microstructure of the alloys after casting is dendritic (Fig. 1). Dendrite cores are formed by channels of the γ phase which surrounds the fine grains of the γ' phase. These clusters look like a mesh. There is the γ' phase between dendrite core and boundary. The casts alloyed with boron contain many pores.

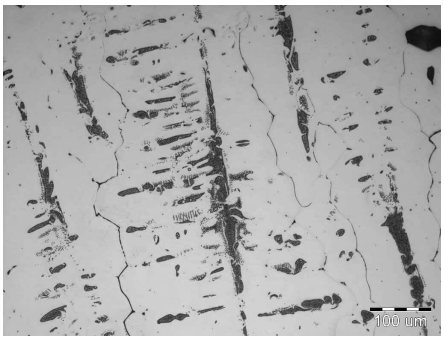

Fig. 1. **Microstructure of Ni-22Al-0.1B alloy (at.%) after cast**

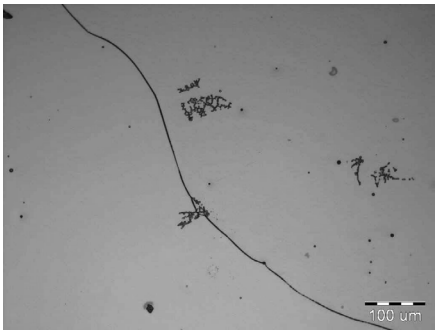

Fig. 2. **Microstructure of Ni-22Al-0.1B alloy (at.%) after directional solidification (V = 50 mm h^{-1})**

After directional solidification, the structure is oriented in a direction of growth (Fig. 2). Grains on the transversal sections are equiaxed and formed by the γ' phase. There are traces of mesh at grain boundaries and also in the centre of grains. Volume fraction of the mesh decreases with increasing boron concentration. Boron does not form individual phases for the used concentrations.

3.2. Porosity

Pore amount in the casts is greater than in the directionally solidified alloys. The alloys contain the pores in sizes from 0.5 to 27.0 μm. For the as-cast and the as-directionally solidified samples, porosity increases together with boron concentration (Tab. I).

The casts contain big and many elliptical pores with rough surface. After directional solidification, amount of big pores decreases. The remaining pores have more circular contour and smoother surface (Fig. 3).

Table I
Porosity of Ni-24Al Alloys without and with Boron

Alloy [at. %]	P_C [%]	P_{DS} [%]
Ni-24Al	0.18 ± 0.10	0.03 ± 0.01
Ni-24Al-0.1B	0.26 ± 0.28	0.12 ± 0.08
Ni-24Al-0.24B	0.33 ± 0.34	0.21 ± 0.21

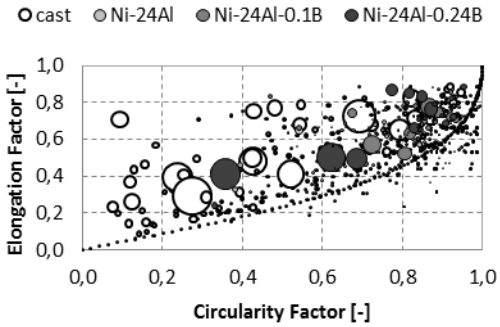

Fig. 3. **Estimation of pore morphology in the samples of Ni-24Al, Ni-24Al-0.1B a Ni-24Al-0.24B alloys (at.%) after cast and after directional solidification**

3.3. Microhardness

Directional solidification process slightly decreases microhardness of the alloys in contrast to cast state. The microhardness of the as-cast and the as-directionally solidified samples increases with increasing boron concentration (Tab. II). The measurement has not confirmed a matrix softening of Ni-24Al alloy by boron alloying.

The presence of boron at grain boundaries has been indirectly confirmed by the microhardness measurement carried out from boundary to the centre of grains (Fig. 4). Alloy microhardness measured by this way always decreases. In this case, the hardest alloy is the one with 0.24 at.% of boron and the weakest alloy is the unalloyed one.

4. Conclusions

The measurements carried out in this paper have confirmed that alloying and process of directional solidification affect microstructure, porosity and microhardness of Ni-24Al, Ni-24Al-0.1B and Ni-24Al-0.24B alloys (at.%).

As-directionally solidified alloys have an oriented microstructure which is formed by elongated grains of the γ' phase parallel to the direction of the growth. They have smaller number of pores with smother surfaces and lower microhardness that the as-cast alloys.

The effect of boron alloying on matrix softening of Ni-24Al alloy has not been confirmed.

Table II
Microhardness of Ni-24Al Alloys without and with Boron (the HV load value is 50 g)

Alloy [at. %]	HV_C 0.05 [-]	HV_{DS} 0.05 [-]
Ni-24Al	244 ± 26	228 ± 20
Ni-24Al-0.1B	254 ± 43	245 ± 12
Ni-24Al-0.24B	273 ± 41	255 ± 11

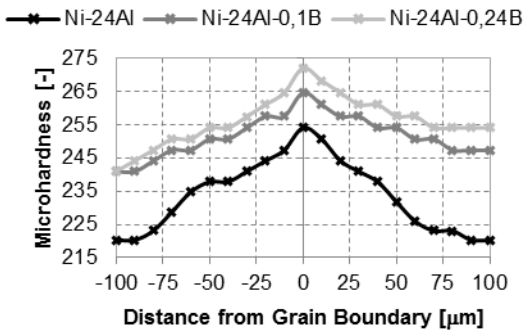

Fig. 4. **Decrease of microhardness in Ni-24Al, Ni-24-0.1B and Ni-24Al-0.24B alloys (at.%) from grain boundary to grain centre**

The presented results were obtained within the frame of solution of the state budget of the Czech Republic and project MSM 6198910013 "Processes of preparation and properties of high-purity and structurally defined special materials".

REFERENCES

1. Stoloff N. S.: Int. Mater. Rev. *153*, 34 (1989).
2. Jiating G., et al.: Mater. Sci. Eng. *120*, A152 (1992).

M. Pohludka, J. Malcharcziková, and M. Kursa *(VŠB – Technical University of Ostrava):* **Microstructure and Properties of the Ni-Al-B Alloys after Directional Solidification**

Ni-24Al, Ni-24Al-0.1B and Ni-24Al-0.24B alloys (at. %) were prepared by vacuum induction melting and by directional solidification at the rate of 50 mm/h and at the 1550 °C. After directional solidification, alloy microstructure consists of elongated grains of the γ' phase. Alloy matrix also contains small amount of the γ phase. There are no boron phases in these alloys. Process of directional solidification decreases an amount of the pores which the alloys contain after cast and modify their morphology. Microhardness of the alloys after directional solidification is lower then microhardness of the alloys after cast. However, there is no matrix softening of Ni-24Al alloy as a result of boron alloying.

LOCAL MICROMECHANICAL PROPERTIES OF DENTAL COMPOSITES

ONDŘEJ PREJZEK, JOSEF ŠEPITKA, JAROSLAV LUKEŠ, and MIROSLAV ŠPANIEL

Czech Technical University in Prague, Faculty of Mechanical Engineering, Dept. of Mechanics, Biomechanics and Mechatronics, Technicka 4, 166 07 Prague, Czech Republic
Ondrej.Prejzek@fs.cvut.cz

Keywords: nanoindentation, dental composites, elastic modulus, reduced modulus

1. Introduction

A detailed knowledge of elastic properties of dental restorative materials is essential for obtaining reliable computational models for an optimization of a mechanical performance. Many works deal with measurement of the elastic modulus of dental composites, but the results vary, depending on the measurement method. In the case of an uniaxial test, moduli measured under tensile load are referred to be significantly higher, than those measured under compressive direction[1–3]. This work has following aim: it maps the elastic moduli of dental composites composed of glass particles and polymer resin, as well as individual constituents. Consecutively, moduli are compared with the moduli previously measured by an uni-axial compressive test. Additionally to each elastic modulus measurement, the value of indentation hardness H_{IT} was determined.

2. Materials and methods

Three commercially available composite materials have been subjected to an experiment. Opticor Flow (SpofaDental a.s., Jičín, Czech Republic), Filtek Z250 (3M ESPE, St.Paul, MN, USA) and Charisma Opal (Heareus Kulzer GmbH, Hanau, Germany). All three materials consist of polymeric resin and glass particles.

2.1. Specimen preparation

The samples are of cylindrical shape (ø 6 × 12 mm), identical to those of samples subjected to compressive experiments. The curing of a specimen has been performed in both radial and axial direction in order to ensure curing of entire volume of the composite. Samples had been cured in a thin plexi tube and thereafter all three samples were put in one mounting cup, embedded in transparent Epofix (Struers GmbH) and polished before the indentation measurement.

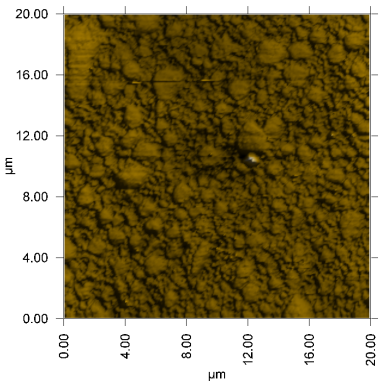

Fig. 1. **Specimen surface (Filtek), obtained by *in-situ* SPM**

2.2. Testing conditions

Quasistatic load controlled experiments were performed with Hysitron TriboIndenter™ system with Berkovich diamond tip.

Time increments of three applied loading steps – increase of loading force, constant loading force, unloading – have been prescribed as 5 × 2 × 5 s. A unique loading force P_{max} has been chosen for each material, in order to meet the indentation depths $h_c > 20$ nm. For the selected materials, $P_{maxCharisma} = 80$ µN, $P_{maxFiltek} = 120$ µN, $P_{maxOpticor} = 50$ µN. Based on standard tip shape calibration on fused quartz we know, that indentation size effect is present up to contact depth 20 nm.

Two experimental procedures have been employed to determine the location of indents:

1. To measure overall modulus of the composite, indentation of a representative area, selected from an optical microscopic image has been utilized. Indents have been applied in square pattern of 8 by 8 with mutual distance of 2 µm, hence in area of 14 by 14 µm.
2. Indentation by piezo-automation method using an image from *in-situ* scanning probe microscopy (SPM) has been used to measure properties of individual constituents. Sample surface has been scanned with a constant force of 2 µN at a scan size 5 by 5 µm in order to distinguish between phases indented afterwards.

3. Results and discussion

For all examined composite materials, the Poisson's ratio of ν = 0.17 (particle) and ν = 0.35 (resin), respectively, was used for the calculation of elastic moduli[4].

All sets of results refer Filtek Z250 being the material with both highest elastic modulus and indentation hardness. Charisma Opal is, in all cases, the material with medium values and Opticor Flow shows lowest values of both modulus and hardness. The order is equal to that observed by results of the compressive test. Compared to results from compressive test, modulus obtained by nanoindentation reaches significantly higher values. This fact can be attributed to the microstructural irregularity of the composite, that does not allow the standard mixing laws[5,6] to be utilized for calculation of global properties of the composite from known properties of constituents. Plastic microstructural residual stress[7] in certain resin regions can also contribute to the decreased elastic modulus measured in compression.

4. Conclusions

Aforementioned results show locally measured properties of three materials measured by two various nanoindentation approaches. Sequence of results by materials is the same for overall moduli, obtained by the optical microscopy approach as well as the moduli of individual constituents, obtained using the piezo-automation approach. This is also valid for the results of the compressive macroscopic measurement; however those values are distinctively lower. This fact implies careful selection of a method to obtain material properties for each particular case of application. The locally obtained values of moduli can be successfully employed to describe local properties, and their change within one specimen, i.e. gradient. However, to describe overall properties of a composite material with a complex microstructural topography, the locally measured results must be subjected to a homogenization procedure, such as FE analysis of structure's overall performance.

Table I
Indentation of area selected from optical microscopy: averaged values of measured properties

Sample	Charisma	Filtek	Opticor
Contact depth [nm]	39.1± 7.4	39.6±7.8	38.7± 8.7
Reduced modulus [GPa]	15.6±3.0	20.1±2.7	8.4±2.5
Elastic modulus [GPa]	13.9±2.6	17.9±2.4	7.42±2.2
Hardness [GPa]	0.5±0.3	1.4±0.4	0.5±0.2

Table II
Piezo automation method: properties of constituents

Sample	Charisma	Filtek	Opticor
Elastic modulus Filler [GPa]	20.8±2.8	30.1±2.9	9.9± 3.3
Elastic modulus Resin [GPa]	10.4±0.1	14.3±1.4	5.2±0.7
Hardness Filler [GPa]	2.54±0.7	3.2±0.6	0.6±0.3
Hardness Resin [GPa]	0.87±0.06	1.50±0.04	0.45±0.04

Table III
Values of elastic modulus, obtained by compressive test

Sample	Charisma	Filtek	Opticor
Compression [GPa]	3.2±0.5	3.4±0.6	1.8±0.3

This work was supported by the Grant Agency of the Czech Technical University in Prague, grant No. SGS10/247/OHK2/3T/1212 and by the Ministry of Education project: Transdisciplinary research in Biomedical Engineering II, No. MSM 6840770012.

REFERENCES

1. Kleverlaan C.J., et al.: Dent. Mat. *2*, 1150 (2005).
2. Beatty M. W., et al.: Biomaterials *14*, 999 (1993).
3. Pidaparti, R. M. V., et al.: Eng. Fra. Mech. *45*, 51 (1993).
4. Oliver W. C., Pharr G., G.M.: J. Mater. Res. *7*, 1564 (1992).
5. Voigt W.: Ann. Phys. Chem. *274*, 573 (1889), (in German).
6. Reuss A.: ZAMM *9*, 49 (1929) (in German).
7. Harris B.: J. Mater. Sci. *13*, 173 (1977).

O. Prejzek, J. Šepitka, J. Lukeš, and M. Španiel *(Czech Technical University in Prague, Faculty of Mechanical Engineering, Dept. of Mechanics, Biomechanics and Mechatronics, Czech Republic):* **Local Micromechanical Properties of Dental Composites**

The paper deals with nanoindentation measurement of local properties (elastic modulus and indentation hardness) of three dental composite materials. Properties of particular phases of the material, filler particles and resin, respectively, were measured by a piezo-automation approach. To obtain overall properties of the composite, indentation of locations, selected from an optical microscopic image has been performed. Obtained results are compared with data, previously gained by the uni-axial compressive test. Elastic moduli, obtained locally by nanoindentation are higher, when compared with those, measured globally under compressive load. For the elastic modulus, the order of results, measured for particular materials, remains unchanged by various measurement methods and is equal to that of indentation hardness.

EXPERIMENTAL TECHNIQUES FOR THE MICROSTRUCTURAL CHARACTERIZATION OF RETAINED AUSTENITE STABILITY AND SINGLE PHASE PROPERTIES IN LOW-ALLOYED TRIP-STEELS

HENDRIK QUADE[a], ANDRE STEFFEN[b], PETRA GAVENDOVÁ[c], ULRICH PRAHL[a], METIN TOLAN[b], and WOLFGANG BLECK[a]

[a] *Department of Ferrous Metallurgy at RWTH Aachen University, Intzestraße 1, 52072 Aachen, Germany,*
[b] *Fakultät Physik/DELTA, TU Dortmund, Maria-Goeppert-Mayer-Str. 2, 44227 Dortmund, Germany,*
[c] *Institute of Materials Research, SAS, Watsanova 47, 040 01 Košice, Slovakia*
hendrik.quade@iehk.rwth-aachen.de

Keywords: TRIP-steels, synchrotron radiation, high-energy X-ray diffraction, electron backscatter diffraction, nano indentation, phase transformation

1. Introduction

TRIP-steels are subjected to a high attention for the application of automotive parts, because they exhibit a high formability at a given strength level.

It was found that high energy synchrotron X-ray diffraction is excellently suited for the investigation of the austenite stability[12]. To identify the local distribution of the face-centered cubic phase, electron backscatter diffraction can be a usefull technique, especially for the investigation for the local martensite formation[3].

Typically, low-alloyed TRIP-steels consist of a ferrite matrix with embedded islands of retained austenite, bainite and some martensite (Fig. 1).

Two important mechanisms are responsible for the strain-hardening behaviour of a TRIP-steel: the phase transformation of metastable retained austenite to the much harder phase martensite, and the composite effect of the microstructure due to the presents of several single phases[4]. The locations of the austenitic grains in the microstructure are of major importance because they alter the extent of the phase transformation, the microstructural strain localization and therefore the macroscopical formability of the steel[5].

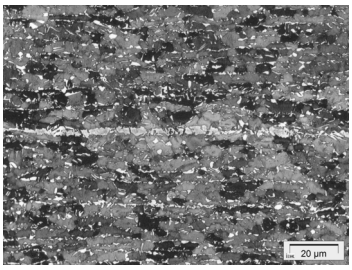

Fig. 1. **Light optical image of a TRIP microstructure after Klemm etching**

2. Materials and methods

The investigations were carried out for three industrial TRIP-steels named TRIP A, B (Rm = 700 N mm^{-2}) and TRIP C (Rm = 800 N mm^{-2}) based on different chemical compositions (Table I). The engineering stress-strain curves can be seen in Fig. 2. TRIP A and B exhibit nearly the same strain hardening and fracture strains were TRIP C has the highest tensile strength due to the highest silicon content, because silicon is a strong ferrite strengthening element.

Synchrotron high energy X-ray diffraction experiments were performed at the beamline BL9 of the Dortmunder Elektronenspeicherring-Anlage (DELTA) in order to study the transformation kinetics in-situ as a function of applied tensile force. The left image of Fig. 3 shows the appeared Debye-Scherrer rings after radiography of a TRIP-steel sample, where each ring belongs to a certain plane of the crystal lattice.

The existence of full Debye-Scherrer rings over the whole 360° indicate that the material exhibits no significant texture in the undeformed state. The disappearance of the peaks corresponding to the {111},{200} and {220} plane of the austenitic phase during straining is a proof for

Table I
Chemical composition of the investigated steel grades

[wt.%]	C	Mn	Si	Al	P
TRIP A	0.165	1.67	0.341	1.10	0.093
TRIP B	0.179	1.77	0.039	1.61	0.014
TRIP C	0.205	1.68	1.63	0.039	0.016

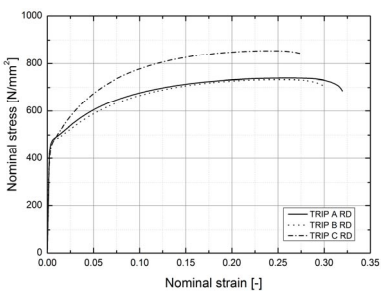

Fig. 2. **Engineering stress strain curves of the investigated TRIP-steels** (gauge length = 80 mm)

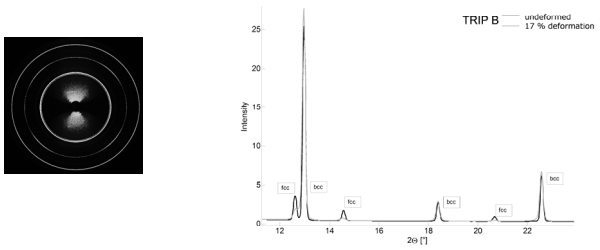

Fig. 3. **Arisen Debye-Scherrer rings after radiography of the sample (left), corresponding diffractogram (right)**

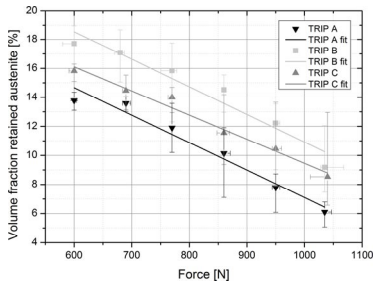

Fig. 5. **Volume fraction of retained austenite as a function of applied tension force determined by synchrotron experiments**

a phase transformation in the sample. The calculation of the volume fraction was carried out by using the evaluation software Maud[6] (Materials Analysis Using Diffraction).

In order to investigate the local, morphological influence on the martensite formation, electron backscatter diffraction was used. Therefore a scanning electron microscope JEOL JSM7000F in combination with an EBSD-detector was applied. A measuring field of 50 μm × 50 μm and a step-size of 60 nm for the readout of the EBSD pattern were chosen. To create a connection with the local plastic deformation on the sample the true strains were measured by the usage of a Vialux Autogrid® system (Fig. 4).

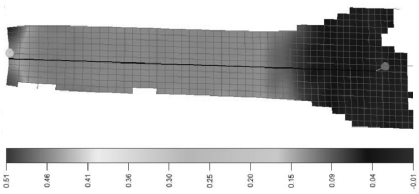

Fig. 4. **Distribution of true equivalent plastic strain on a cracked sample measured by means of Vailux Autogrid® system**

For the determination of the strength of the ferritic phase, nanoindentations were conducted on a Nano Indenter® G 200 by the usage of a pyramidal diamond Berkovich indenter tip. The tests were carried out according to the standard norm[7], where the indentations were done with a maximum force of 5 mN. In order to minimize the measurement error and to achieve representativeness, 50 indentations were performed and for the determination of the hardness modulus a Poissons's ratio of 0.3 was assumed.

3. Results

Fig. 5 shows the austenite volume fractions as a function of applied tension force and nominal strain, determined by the X-ray diffraction experiments. Under consideration of the tensile force it has to be mentioned that all 3 steels show a nearly equal austenite stability, where the highest is presented in TRIP C and the lowest in TRIP B.

Regarding the strains, two regimes were observed, where a massive transformation takes place at the onset of yielding and low states of deformation and a regime at higher strain values were the martensite formation reaches a saturation due to a decrease of availability of possible transformation nucleation sites (Fig. 6). The transformation kinetics stay in close correlation with the development of the strain hardening values over engineering strain. The local transformation kinetic is among other factors influenced by the arrangement of the retained austenite grains in the microstructure which changes over the thickness of the sheet. The phase distribution varies from a nearly homogeneous at one third thickness to an inhomogenous banded dispersion of the second phases at the sheet centre in TRIP steel B. In addition, initial thermal martensite was detected which cannot serve for a TRIP-effect at the beginning of straining of the material (Fig. 7). These martensite bands are a consequence of segregations in the steel sheet, were an enrichment of manganese in these regions was observed.

In order to achieve information about the impact of the local loading condition on the martensite formation the

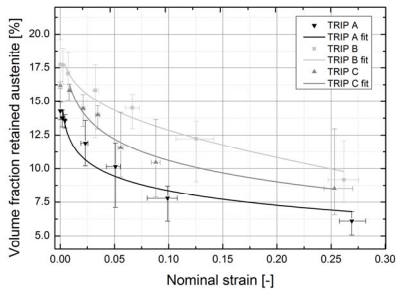

Fig. 6. **Volume fraction of retained austenite as a function of engineering strain determined by synchrotron experiments**

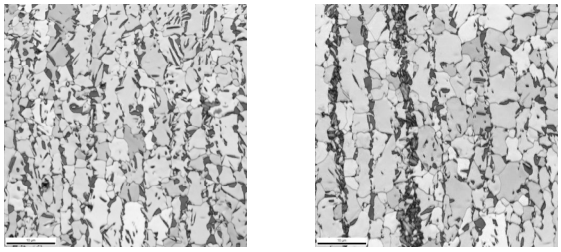

Fig. 7. **Alteration of the morphology over the sheet thickness in TRIP B (left: homogeneous distribution of retained austenite at one third position, right: heterogeneous distribution of the retained austenite in combination with a centred martensite band at sheet centre)**

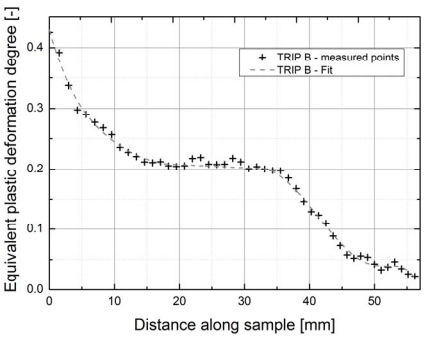

Fig. 8. **True equivalent plastic strain along the tensile sample in TRIP B measured by means of Vialux Autogrid® system**

local stress-strain conditions have to be known. Fig. 8 depicts the magnitude of equivalent plastic strain from the fracture of an investigated tensile sample to the clamping region.

Highest values occur close to the crack due to the strain localization and necking where a plateau is observable in the regions of uniform deformation.

Based on this knowledge the evolution of the phase fractions of retained austenite as a function of the local true equivalent plastic strain with the same trend as acquired by the synchrotron experiments can be seen in

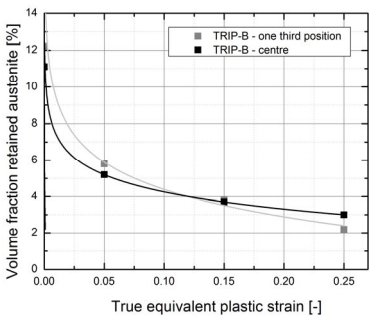

Fig. 9. **Volume fraction of retained austenite determined by electron backscatter diffraction in TRIP B**

Fig. 9. It was found that martensite formation upon deformation of the material takes place only partially within the grains in dependence on the local position in the microstructure and chemical composition.

The ferritic matrix in the investigated steels has a different strength which itself offers a resistance against the volume dilatation accompanying the martensite formation (Fig. 10). The differences in the hardness values are mainly due to the different contents of silicon. Typically, silicon and aluminium are alloyed for the prevention of carbide precipitation during isothermal holding. But additionally silicon has a strong influence on the ferrite strength were the tensile strength increases by approximately 50 MPa per 0.5 wt.% (ref.[8]).

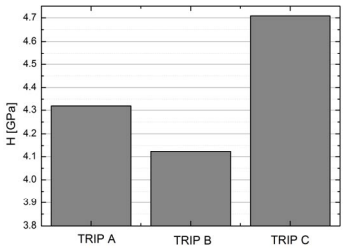

Fig. 10. **Hardness of the ferritic phase determined by nanoindentation**

4. Conclusions

The morphology strongly influences the phase transformation were the martensite formation only partially takes place within austenitic grains. 3 types of local retained austenite morphologies were observed in certain regions of the investigated steel sheets: a homogeneous distribution, an arrangement of austenite particles in bands and retained austenite particles located in a martensitic band.

These different types of microstructural phase distribution leads to an alteration of the local TRIP-effect and therefore mechanical properties.

Not only the retained austenite stability but also the strength of the ferritic matrix plays an important role for the mechanical properties of the entire composite.

This research was carried out under the Project No. MC2.07293 in the framework of the Research Program of the Materials innovation institute M2i (http://www.m2i.nl).

REFERENCES

1. N. Jia, Z. H. Cong, X. Sun, S. Cheng, Z. H. Nie, Y. Ren, P. K. Liaw, Y. D. Wang: Acta Materialia *57*, 3965 (2009).
2. N. H. van Dijk, A. M. Butt, L. Zhao, J. Sietsma, S. E. Offerman, J. P. Wright, S. van der Zwaag: Acta Materialia *53*, 5439 (2005).

3. S. Zafferer, P. Romano, F. Friedel: J. Microscopy *230*, 499 (2008).
4. P. Jacques: *PhD-thesis*, Université catholique de Louvain, Département des sciences des matériaux et des procédés, 1998.
5. H. Quade, U. Prahl, W. Bleck: Chem. Listy *105*, s705 (2011).
6. L. Lutterotti, M. Bortolotti, G. Ischia, I. Lonardelli, H.-R. Wenk: Z. Kristallogr., Suppl. *26*, 125 (2007).
7. DIN-EN ISO 14577-1, Metallic materials – Instrumented indentation test for hardness and materials parameters – Part 1, 2003.
8. F. B. Pickering: *Physical Metallurgy and the Design of Steels*, London, U.K.: Applied Science, 1978.

H. Quade[a], A. Steffen[b], P. Gavendová[c], U. Prahl[a], M. Tolan[b], and W. Bleck[a] *([a] Department of Ferrous Metallurgy at RWTH Aachen University, Aachen, Germany, [b] Fakultät Physik/DELTA, TU Dortmund, Dortmund, Germany, [c] Institute of Materials Research, SAS, Košice, Slovakia):* **Experimental Techniques for the Microstructural Characterization of Retained Austenite Stability and Single Phase Properties in Low-Alloyed TRIP-Steels**

The present work deals with experimental facilities for the characterization of low-alloyed TRIP-steels in terms of the phase transformation and the local mechanical properties of the microstructure. The TRIP-effect is a complex phenomenon which acts locally. An evaluation of the deformation-state in the sheet plane by the usage of a measurement system Vialux Autogrid® gives information about the impact of the local stress-strain condition on the phase transformation. In addition, there exists a further locality effect which becomes noticable over the sheet thickness. Due to industrial boundary conditions, the morphology changes from a homogeneous distribution to a banded arrangement of the second phases. To investigate this local influence, the electron backscatter diffraction technique seems to be a feasible tool. Besides the retained austenite stability, the ferritic phase has a major influence on the behaviour of the overall steel grade. To characterize the strength of the ferrite matrix it was proven that nano indentation is a practical method.

NANOWEAR TESTING OF COMPOSITE MATERIALS

RADEK SEDLÁČEK[a], TOMÁŠ SUCHÝ[a,b], JOSEF ŠEPITKA[a], JAROSLAV LUKEŠ[a], MIROSLAV SOCHOR[a], KAREL BALÍK[b], ZBYNĚK SUCHARDA[b], and JAN BENEŠ[c]

[a] *Czech Technical University in Prague, Fac. of Mech. Eng., Technická 4, Prague 6, 166 07,* [b] *Institute of Rock Structure and Mechanics, ASCR, v.v.i., V Holešovičkách 41, Prague 8, 182 09,* [c] *Medin, Inc., Vlachovická 619, Nové Město na Moravě, 592 31, Czech Republic*
radek.sedlacek@fs.cvut.cz

Keywords: nanoindentation, wear, mechanical properties, polymeric composite, sterilization

1. Introduction

Radiolucent composite materials have properties superior to those of insufficiently radiolucent metal alloys and unreinforced polymers with poor mechanical properties. The steam or dry heat sterilization processes widely employed in medical practice can affect the micromechanical properties of polymeric composites, particularly in the interface region between the matrix and the reinforcing fibers[1]. The structural integrity and the overall performance of fiber-reinforced polymer composites are strongly influenced by the stability of the fiber/polymer interfacial region[2]. It is necessary to investigate both the microscopic and the macroscopic changes in mechanical and structural properties due to the sterilization processes that are employed. The aim of this study was to verify a methodology for assessing the influence of multiple sterilization processes on the inner structure of composites.

2. Materials and methods

Composite materials (C/PPS) based on carbon T300 fibers (plain weave fabrics, Toray, Japan) and polyphenylenesulfide (TenCate, Holland) matrix were prepared. The C/PPS composite was consolidated under a pressure of 1.0 MPa at 310 °C for 10 min (rate of temperature increase and/or decrease: 10 °C/min). In order to assess the influence of multiple sterilization processes on the inner structure of the composites, mechanical and structural analyses were performed before sterilization (**A**), after 1 sterilization process period (**B1**), and after 30 (**B30**) sterilization process periods. An autoclave (Sterident, Prodenta, CZ) for steam sterilization (134 °C, 304 kPa, 10 min) was used for this purpose.

An assessment of the impact of multiple sterilization processes on the inner structure of the composites was carried out at two levels: macroscale and microscale. The macroscopic behaviour was studied by flexural tests. The ultimate strength in bending and the modulus of elasticity in bending in the direction of the fibers were determined with a four-point and three-point bending set-up (Inspekt 100HT, Hagewald & Peschke, Germany), in accordance with ISO 14125.

The microscopic behaviour was studied by nanoindentation tests. The assessment of the impact of multiple sterilization processes on the inner structure of the composites was studied using ScanningWear ™ mode, a nanomechanical instrument option of Hysitron TriboIndenter™ TI 950. A Berkovich diamond tip with apex radius of ~120 nm was employed for the ScanningWear tests. The tip was raster-scanned across a 40×40 μm area of the sample surface (in close proximity to the fibers) in 256 scan lines with 100 μN contact force for 5 passes. Immediately after each wear test had been completed, the worn areas were imaged using a 60×60 μm scan size and a 2 μN contact force (scanning probe microscopy, SPM). The nano wear evaluation was carried out in SPIP 5.1.6. software (ImageMetrology, Denmark). The mean values of each worn area were compared with the mean values of the corresponding unworn areas, and the wear depths were calculated.

A statistical evaluation was carried out using the STATGRAPHICS Centurion XV software (StatPoint, USA): the statistically significant differences were checked by nonparametric methods (the Kruskal-Wallis test, α=0.05); the Mann-Whitney test was used as a post hoc test (α=0.05).

3. Results and discussion

The flexural properties after multiple sterilizations were tested and compared with those of the corresponding unsterilized samples (Fig. 1 and Fig. 2). The results and the statistical analysis show that the modulus of elasticity in bending is not influenced by the multiple sterilizations studied here. The values are in reasonable agreement with earlier results obtained by flexure tests in the direction of the reinforcing fibers[3]. In the case of ultimate strength in bending, a statistically significant increase after 1 sterilization process (app. 6.5 %) and after 30 sterilization processes (app. 7.2 %) can be observed. This increase may be explained by equalization of the residual stress development during the consolidation of the composites. The applied sterilization temperature (134 °C) is above the glass transition temperature (T_g) of the fabric reinforced PPS composites. Depending on the staking sequence, the vol-

ume fraction and the reinforcement material of the laminate, the T_g of the fabric composites is about 83–98 °C (ref.[3,4]). The residual stresses created during the processing of thermoplastic-based composites can probably be optimized by further limited application of temperature above T_g. A further increase in temperature above T_g may soften the matrix behaviour and significantly reduce the mechanical properties[3].

The influence of multiple sterilization processes on the inner structure of the composites was further analysed by an evaluation of the stability of the fiber/matrix interfacial region (see Fig. 3). The wear depths of the worn areas after nano scratching were assessed (Fig. 4). The results provide an assessment of the influence of multiple sterilization processes on the inner structure of the composites. The analysis shows that no structural changes occurred in the region close to the fibers, and the stability of the fiber/matrix region was preserved after 30 sterilization processes. For further analyses in our study, it will be necessary to increase the number of sterilization cycles in a manner that simulates the life cycle of widely-used medical devices, e.g. composite parts of a medical targeting system.

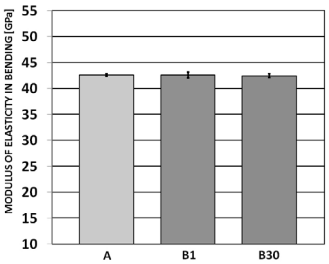

Fig. 1. **Modulus of elasticity in bending before (A), after 1 sterilization process (B1), and after 30 sterilization processes (B30).** There is no statistically significant difference between the values (Mann-Whitney post-hoc test, α=0.05, *n*=6)

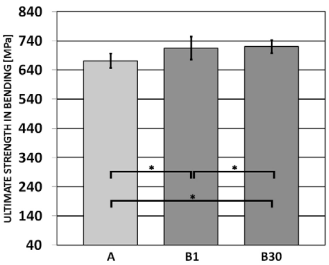

Fig. 2. **Ultimate strength in bending before (A), after 1 sterilization process (B1), and after 30 sterilization processes (B30).** (*denotes statistically significant differences, Mann-Whitney post-hoc test, α=0.05, *n*=6)

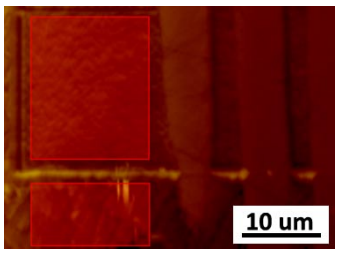

Fig. 3. ***In-situ* SPM micrograph of unworn (rectangle below) and worn (at the top) areas after 10 cycles of ScanningWear.** The fibers are situated on the right side of the micrograph

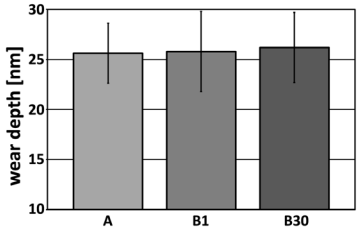

Fig. 4. **Wear depths of worn areas of composites before (A), after 1 sterilization process (B1), and after 30 sterilization processes (B30).** There is no statistically significant difference between the values (Mann-Whitney post-hoc test, α=0.05, *n*=6)

4. Conclusion

On the basis of our analyses, we can state that the C/PPS composite is a good candidate for application as a radiolucent material providing resistance against steam sterilization decomposition. Before it is presented for application, it will be necessary to apply greater numbers of sterilization cycles.

This research was supported by the Czech Science Foundation (project No. 108/10/1457), and by Ministry of Education project Transdisciplinary Research in Biomedical Engineering II, No. MSM 6840770012.

REFERENCES

1. Zheng Q.: J. Comp. Mater. *27*, 1465 (1993).
2. Godara A., Raabe D., Green S.: Acta Biomater. *3*, 1742 (2007).
3. Vieille B., Aucher J., Taleb L.: Adv. Polym. Tech. *30*, 80 (2011).
4. Rebenfeld L., Desio G.P., Wu J.C.: J. Appl. Polym. Sci. *42*, 801 (1991).

R. Sedláček[a], T. Suchý[a,b], J. Šepitka[a], J. Lukeš[a], M. Sochor[a], K. Balík[b], Z. Sucharda[b], and J. Beneš[c]
([a] CTU in Prague; Fac. of Mech. Eng.; [b] Institute of Rock Structure and Mechanics, ASCR, v.v.i.; [c] Medin, Inc.):
Nanowear Testing of Composite Materials

This study evaluates the resistance against multiple steam sterilization of composite materials based on carbon fibers and polyphenylene sulfide matrix. The influence of multiple sterilization processes on changes in their mechanical and structural properties are determined by flexural and nanoindentation tests.

DYNAMIC MECHANICAL PROPERTIES OF SOFT TISSUES LOCALIZED BY FLUORESCENCE MICROSCOPE OBTAINED USING NANOINDENTATION

JOSEF ŠEPITKA[a], JAROSLAV LUKEŠ[a], LIBOR STANĚK[b], and JAN ŘEZNÍČEK[a]

[a] *Czech Technical University in Prague, Faculty of Mechanical Engineering, Dept. of Mechanics, Biomechanics and Mechatronics, Technicka 4, Prague 166 07,*
[b] *Institute of Pathology, General Faculty Hospital, Charles University, Studnickova 2, Prague 2 128 00, Czech Republic*
Josef.Sepitka@fs.cvut.cz

Keywords: nanoindentation, DMA, fluorescence, soft tissue

1. Introduction

Nanoscale dynamic mechanical analysis (nanoDMA) seems to be an effective tool to obtain material characteristics of biological materials; especially for poorly accessible soft tissues[1,2]. However, we have only basic information on particular tissue localization from an optical microscope, which is attached to an indentation instrument and we are not able to localized separate structures or tissue transitions. This problem can be eliminated by an implementation of fluorescence microscope into a nanoDMA instrument.

The aim of this study was to obtain material characteristics of particular substructure of soft tissues their transition boundaries using a fluorescence microscope for their localization as a part of Hysitron TI 950 TriboIndenter™. The experiments, which are carried out with better understanding of material structure, can clear up a variability of data presented in a biomechanics community.

2. Materials and methods

2.1. Samples preparation

A porcine spine was obtained from a sloughterhouse at the day of testing. The lumbar spine motion segments were immediately dissected and ten millimeter thick plates of vertebral body, end plate and annulus fibrosus were cut under running water condition[2].

For histological investigation, the sample was immediately placed into 10 % buffered. Paraffin-embedded samples were cut into 7–10 μm sections in an angle of 45° to transversal plane using a microtome (Leova). Paraffin was removed with ethanol and xylene (Penta, Czech Republic) and the slices were stained with hematoxylin-eosin (Dako, Denmark). Prepared sample is shown in Fig. 1.

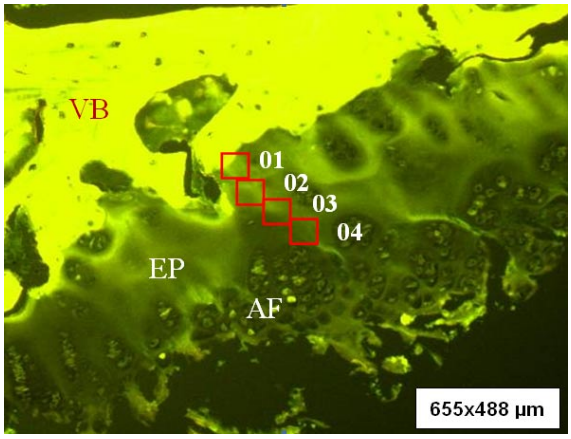

Fig. 1. **Picture obtained by fluorescence microscope shows histological cut which contain vertebral body (VB), endplate (EP) and annulus fibrosus (AF). Red squares denote four indented area**

2.2. Testing conditions

Indents were applied in square pattern of 4 by 4 indents with 15 μm separations. Thus, an area of 45 by 45 μm was characterized by dynamic nanoindentation. Fig. 1 was acquired by built-in flurescence microscope, which clearly shows separate structures and tissue transitions. Red squares 01–04 in the Fig. 1 denote the indented areas. Area 01 represents endplate region close to vertebrae body. Areas 02 and 03 represent central endplate region. Area 04 represents a transition of the endplate and annulus fibrosus.

NanoDMA load controlled experiments were performed with Hysitron TriboIndenter™ system with diamond Berkovich tip. Harmonic loading $P_0 = \sin(\omega t)$ with dynamic load amplitude $P_0 = 30$ μN was specified for the harmonic frequency range 5–200 Hz. During nanoDMA experiment, static load was applied at maximum force $P_{max} = 2000$ μN.

The reduced storage modulus (E_r'), the reduce loss modulus (E_r'') and $\tan\delta = E_r''/E_r'$ dependent on compliance (C_s) and stiffness (K_s) of the sample are given by

$$E_r' = \frac{K_S\sqrt{\pi}}{2\sqrt{A}}, \quad E_r'' = \frac{\omega C_S\sqrt{\pi}}{2\sqrt{A}} \text{ and } \quad \tan\delta = \frac{C_S\omega}{K_S}$$

where A is a projected contact area. The procedure of dynamic nanoindentation according to Asif et al. (1999)[3] is implemented within TriboScan software as well as a calibration procedures and an analysis.

3. Results

Fig. 2 shows that storage and loss moduli are dependent on the frequency. Both moduli increase in all range of the frequency. Fig. 2 shows that average values of storage and loss moduli slowly increase from vertebral bone to annulus fibrosus region (from area 01 to area 04). Fig. 3 shows increasing trend of tan δ within frequency, which represents increasing damping during the experiment.

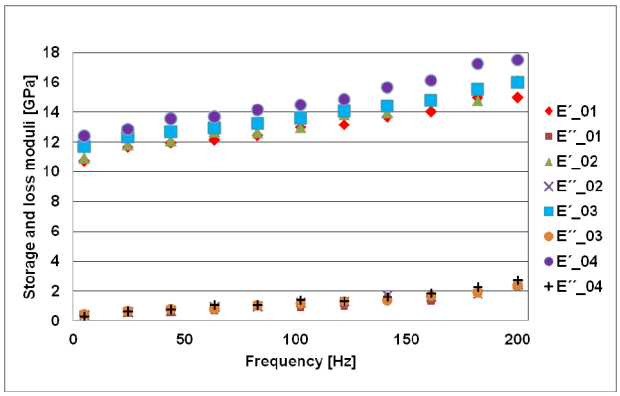

Fig. 2. **Storage (*E´*) and loss (*E´´*) moduli vs. frequency for all tested areas**

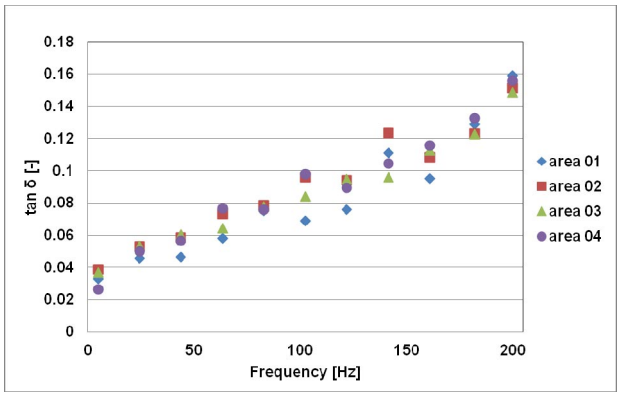

Fig. 3. **Tan δ *vs.* frequency from nanoDMA for all tested areas of the sample**

4. Discussion

Increasing trend of tan δ also indicates increasing amount of dissipation of deformation energy. In other words, viscose element represented by loss moduli increase faster than storage moduli with a strain rate and influences the mechanical behavior of the tissue. We cannot find any slope change in the tan δ trends (Fig. 3) that is usually characterized by an inflection points. Inflection points represent critical values of stiffening (decrease of tan δ) or localized softening (increase of tan δ) of the sample material. It is a question if we can find inflection points in wider range of the frequency as was shown for the cartilage?[1] Analyzed sample seems to be softer with increasing frequency which means that dried endplate has an ability to dissipate more energy at higher frequencies at our frequency range.

5. Conclusions

We obtained local dynamic mechanical properties of a dry porcine intervertebral endplate, which were stained with hematoxylin-eosin, localized by fluorescence microscope using nanoindentation. The combination of both methods shows that we are able to localize and describe particular tissues and their transitions. Damping of the endplate increases during the experiment without critical values of stiffening or localized softening. NanoDMA method is the fastes way of measuring the material characteristics dependent on loading rates. Our end plate sample showed clear dependence on loading rate represented by ramping frequency.

This work was supported by the Grant Agency of the Czech Technical University in Prague, under the project no. SGS10/247/OHK2/3T/12.

REFERENCES

1. Sepitka J., Otahal M., Lukes J.: Comput Method Biomech. *14*, 265 (2011).
2. Sepitka J., Lukes J., Kuzelka J., Rezníček J.: Chem. Listy. *105*, s844 (2011).
3. Asif S. A. S., Wahl K. J., Colton R. J.: Rev. Sci. Inst. *70*, 2408 (1999).

J. Šepitka[a], J. Lukeš[a], L. Staněk[b], and J. Řezníček[a]
([a] Czech Technical University in Prague, Faculty of Mechanical Engineering, Dept. of Mechanics, Biomechanics and Mechatronics, [b] Institute of Pathology, General Faculty Hospital, Charles University, Czech Republic): **Dynamic Mechanical Properties of Soft Tissues Localized by Fluorescence Microscope Obtained Using Nanoindentation**

The paper deals with an assessment of material characteristics of particular substructure of soft tissues their transition by mean of fluorescence nanoindentation.

Ten millimeter thick plates of native lumbar spine motion segments were dissected from sagittaly halved porcine spine. 7–10 µm sections were cut in an angle of 45° to transversal plane using a microtome. They were stained with hematoxylin-eosin afterwards. We obtained dependancies of storage and loss moduli on the frequency range 5–200 Hz. Damping trends and viscosity were discussed in this paper as well.